Biochemistry

Incorporating a Thiophosphate Modification into a Common RNA Tetraloop Motif Causes an Unanticipated Stability Boost

Pradeep S. Pallan, Terry P. Lybrand, Mark K. Schlegel, Joel M. Harp, Hartmut Jahns, Muthiah Manoharan, and Martin Egli*

Read Online

ACCESS | Metrics & More | Article Recommendations | Supporting Information

ABSTRACT: GNRA (N = A, C, G, or U; R = A or G) tetraloops are common RNA secondary structural motifs and feature a phosphate stacked atop a nucleobase. The rRNA sarcin/ricin loop (SRL) is capped by GApGA, and the phosphate p stacks on G. We recently found that regiospecific incorporation of a single dithiophosphate (PS2) but not a monothiophosphate (PSO) instead of phosphate in the backbone of RNA aptamers dramatically increases the binding affinity for their targets. In the RNA:thrombin complex, the key contribution to the 1000-fold tighter binding stems from an edge-on contact between PS2 and a phenylalanine ring. Here we investigated the consequences of replacing the SRL phosphate engaged in a face-on interaction with guanine with either PS2 or PSO for stability. We found that PS2⋯G and Rp-PSO⋯G contacts stabilize modified SRLs compared to the parent loop to unexpected levels: up to 6.3 °C in melting temperature T_m and −4.7 kcal/mol in $\Delta\Delta G°$. Crystal structures demonstrate that the vertical distance to guanine for the closest sulfur is just 0.05 Å longer on average compared to that of oxygen despite the larger van der Waals radius of the former (1.80 Å for S vs 1.52 Å for O). The higher stability is enthalpy-based, and the negative charge as assessed by a neutral methylphosphonate modification plays only a minor role. Quantum mechanical/molecular mechanical calculations are supportive of favorable dispersion attraction interactions by sulfur making the dominant contribution. A stacking interaction between phosphate and guanine (SRL) or uracil (U-turn) is also found in newly classified RNA tetraloop families besides GNRA.

Sarcin/Ricin rRNA GApGA Tetraloop

PO2	PSO	Rp-PSO	Sp-PSO	PS2
58.1°C	63.6°C	64.4°C	59.1°C	63.4°C
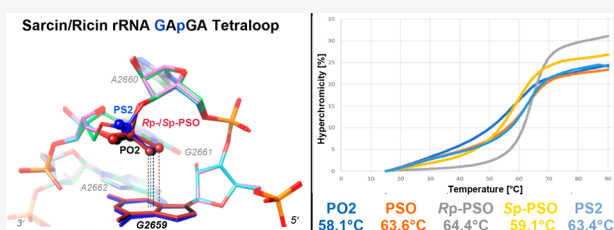
In addition to standard $\pi-\pi$ base stacking and canonical as well as noncanonical base pairing, the expansive fold space of RNA comprises ubiquitous base−backbone and backbone−backbone interactions.[1−6] Not surprisingly, the ribose 2′-hydroxyl group (2′-OH) plays a central role in the formation of the latter. Thus, pairings between 2′-OH groups and 2′-OH and phosphate groups can mediate close contacts between backbone regions, either with or without intermediary water molecules.[7−10] Potential Coulombic repulsion as a result of closely spaced phosphates can be mitigated by nearby 2′-OH groups or metal ions, most commonly Na+, K+, or Mg2+.[11−15]

Various steric and stereoelectronic effects that involve the 2′-OH constrain the ribose conformation (the north C3′-*endo* pucker type is normally favored relative to the south C2′-*endo* pucker type), thereby influencing backbone geometry and direction.[16−20] Moreover, the particular orientation of the 2′-OH moiety, i.e., the position that the hydrogen occupies as a result of a rotation around the C2′−O2′ bond, may play an important role in the RNA tertiary structure.[21]

Another type of RNA backbone−base interaction involves the 4′-oxygen of the ribose stacked onto a nucleobase. This so-called lone pair−π (lp−π) contact, first described a quarter of a century ago for 2′-deoxycytidine O4′ and the adjacent guanine base at CpG steps in left-handed Z-DNA,[22] is widespread in the three-dimensional (3D) structures of RNA molecules.[23] By

comparison, a negatively charged phosphate group stacked onto a base moiety may seem more unusual.[24,25] However, such an interaction is a conserved feature in so-called GNRA tetraloops (N = A, C, G, or U; R = A or G), frequently occurring structural motifs in RNA that closely resemble the uridine turn (U-turn) with a UNR (N = any nucleotide; R = G or A) consensus sequence.[26,27] A prominent example of a GNRA U-turn motif is contained in the rRNA sarcin/ricin loop [SRL (Figure 1a,b)], a highly conserved element in the ribosomal large subunit with the tetraloop sequence GAGA (nucleotides 4323−4326, rat 28S rRNA,[28] and nucleotides 2659−2662, *Escherichia coli* 23S rRNA[29,30]). The rRNA purine-rich 12-nucleotide sequence AGU AC**G AGA** GGA, including the tetraloop (underlined), is universally conserved.[31] The cytotoxin α-sarcin cleaves the phosphodiester bond between G2661 and A2662 (*E. coli* numbering), and ricin depurinates A2660 in the SRL, thereby completely

a)

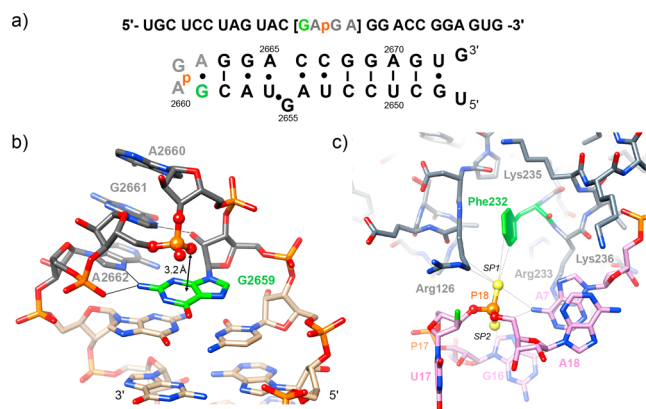**5'- UGC UCC UAG UAC [GApG A] GG ACC GGA GUG -3'**

b)

c)

Figure 1. (a) Sequence and secondary structure and (b) tertiary structure (PDB entry 3DVZ[29]) of the *E. coli* 23S rRNA SRL. Selected residues are numbered, and the phosphate group of G2261 and carbon atoms of the base of G2259 that engage in an lp−π contact are highlighted in ball-and-stick mode and light green, respectively. (c) Edge-on PS2−phenyl contact (shortest distance, 3.7 Å) in a modified RNA aptamer:thrombin complex.[36] Selected residues are labeled. The PS2 moiety and carbon atoms of Phe232 are highlighted in ball-and-stick mode and light green, respectively, and hydrophobic as well as H-bonding interactions are shown with thin lines.

inactivating the ribosome.[32] Because GNRA tetraloops are thermodynamically particularly stable relative to other loop sequences, the phosphate−base stacking interaction may not be merely tolerated but actually energetically favorable.

We recently observed that regiospecific incorporation of a dithiophosphate moiety (PS2) in place of phosphate (PO2) into the backbones of RNA molecules (e.g., viral RNA and siRNA) resulted in dramatically improved binding affinities of the complexes with their respective target proteins.[33−35] Antithrombin and anti-VEGF RNA aptamers with a single PS2 exhibited a K_d of ∼1 pM or 1000-fold tighter than that of the corresponding native RNAs with thrombin and VEGF-165, respectively.[36] Interestingly, monothiophosphate (PSO) incorporation at the same sites resulted in a much more modest gain (thrombin) or an actual loss (VEGF) of binding affinity. Comparison of the crystal structures of complexes between thrombin and the PS2-modified and native RNA aptamers revealed a local RNA-induced fit in the former that produced a close contact between a PS2 sulfur atom and the edge of the phenyl ring from thrombin Phe-232 (Figure 1c). Quantum mechanical (QM) and QM/molecular mechanical (MM) calculations support the conclusion that a close edge-on PS2−benzene contact is energetically favorable compared to the one involving PO2. In addition, the calculations demonstrated that disparate polarization and dispersion energies between the PO2 and PS2 complexes are key to the difference in binding affinity.[37]

In the thrombin aptamer complex, the dramatic gain in affinity chiefly results from an edge-on interaction between a PS2 moiety and an aromatic ring. An RNA-induced fit and an electric field around PS2 and phenyl generated by lysines and arginines were other hallmarks of this system. Given the stunning benefits of oxygen → sulfur substitution for RNA−protein binding affinity based on an edge-on interaction with an aromatic side chain, we wished to analyze the consequences of a face-on interaction involving PS2 or PSO stacked on guanine in the RNA tetraloop relative to the parent PO2−base contact for stability. Here, we show that face-on *R*p-PSO···G

and PS2···G stacking stabilizes modified SRLs compared to the native SRL with the GAGA tetraloop by −4.7 and −3.5 kcal mol⁻¹, respectively ($\Delta\Delta G°$), that the vertical distance to the guanine plane for sulfur is practically the same as for oxygen in SRL crystal structures, and that the stabilizing effect is mainly due to an attractive dispersion interaction. Conversely, introduction of a neutral 2-deoxy-A-methylphosphonate (dAMePO) modification into the SRL did not lead to a significant stabilization compared to the parent RNA.

■ EXPERIMENTAL PROCEDURES

Oligonucleotide Synthesis and Characterization. Oligonucleotides were synthesized on an ABI-394 DNA/RNA synthesizer at a 5 μmol scale using standard solid phase synthesis and deprotection protocols. A solution of 0.25 M 5-(*S*-ethylthio)-1*H*-tetrazole in acetonitrile (CH₃CN) was used as the activator. The phosphoramidite solutions (commercially available standard RNA amidites) were prepared at a concentration of 0.15 M in anhydrous CH₃CN. The oxidizing reagent was 0.02 M I₂ in a THF/pyridine/H₂O solvent or 100 mM DDTT in a 9:1 pyridine/acetonitrile solvent. The detritylation reagent was 3% dichloroacetic acid (DCA) in CH₂Cl₂. The dAMePO-SRL was synthesized according to previously published protocols.[38]

After completion of the automated synthesis, oligonucleotides were manually released from support and deprotected using 30% NH₄OH and 5% diethylamine for 6 h at 55 °C. After filtration through a nylon syringe filter (0.45 μm), 2′-hydroxyl groups were deprotected by treatment with Et₃N·3HF at 60 °C for 10 min. Oligonucleotides were purified using anion-exchange high-performance liquid chromatography (IEX-HPLC) using an appropriate gradient of the mobile phase (0.15 M NaCl with 10% CH₃CN and 1.0 M NaBr with 10% CH₃CN) and desalted using size-exclusion chromatography with water as an eluent. Oligonucleotides were then quantified by measuring the absorbance at 260 nm using the following extinction coefficients: 13.86 L mol⁻¹ cm⁻¹ for A, 7.92 L mol⁻¹ cm⁻¹ for U, 6.57 L mol⁻¹ cm⁻¹ for C, and 10.53 L mol⁻¹ cm⁻¹ for G.

The purities and identities of the three RNAs were verified by analytical anion-exchange chromatography and mass spectrometry, respectively (Table S1). Separation of the PSO-SRL (Figure S1) or dAMePO-SRL (Figure S2) diastereomers was accomplished using reversed phase HPLC with a gradient of acetonitrile in 50 mM triethylammonium acetate (TEAA) or 100 mM ammonium acetate, respectively. Both separations closely followed previous reports.[38,39] As previously observed, the *R*p-PSO isomer eluted first.[39]

Ultraviolet (UV) Thermal Melting Experiments with PO2-, PSO-, and PS2-SRL RNAs. UV melting curves were recorded using a Cary 4000 Scan UV−visible spectrophotometer. The concentration of the oligonucleotide was 2 μM, and samples were prepared in 1× PBS buffer [137 mM sodium chloride, 2.7 mM potassium chloride, 8 mM sodium phosphate dibasic, and 2 mM potassium phosphate monobasic (pH 7.4)]. Samples were annealed by being heated to 85 °C and then slowly cooled to 15 °C. For T_m measurements, samples were then heated to 90 °C at a gradient of 0.2 °C/min, and the change in UV absorbance at 260 nm was recorded. The melting temperature was calculated from the first derivative of the melting curve (Figure S3). All experiments were carried out in at least triplicate.

Calculation of Thermodynamic Parameters. We followed the approach developed by Marky and Breslauer[40] to calculate thermodynamic parameters based on the UV melting curves. (i) Using the graphic analysis shown in Figure 1 of their paper, we calculated lower baselines, upper baselines, and α curves (Figures S4–S6, respectively) from the melting curves (Figure S3). Not unexpectedly, the α curve shapes are different for the PO2, PSO, and PS2 oligos, as was already apparent from the melting profiles. Next, we computed ΔH_{vh} values using eq 4a, whereby $2 + 2n$, the leading coefficient for a monomolecular process, is 4, R is 1.98 cal mol^{-1} K^{-1}, the T_m is the T at $\alpha = 0.5$, and $d\alpha/dT$ is the slope as shown in Figure S7. Then eq 14 provided the values for $\Delta G°$ at 298.15 °C: $\Delta H_{vh}(1 - T/T_m) = \Delta G°$. Finally, the Gibbs free energy under standard conditions just calculated together with ΔH_{vh} (independent of temperature) gave the values for $\Delta S°$ as per eq 13 in ref 40 (Table S2). T_m values and thermodynamic parameters for SRLs with dAPO2, dAPSO, or dAMePO moieties in the SRL loop are shown and listed in Figures S9–S12 and Tables S4 and S5, respectively.

Crystallization, X-ray Data Collection, Phasing, and Refinement. PSO-, PS2-, and Sp-MePO-SRL RNAs were dissolved in a buffer solution composed of 1 mM sodium EDTA (pH 8.0) and 10 mM Tris-HCl (pH 8.0) to a concentration of 350 μM. RNAs were annealed by being heated to 65 °C for 2 min and then slowly cooled to room temperature and stored overnight at 4 °C. Crystallization setups were made by mixing 4 μL of an RNA solution with 2 μL of a crystallization buffer composed of 3.0 M ammonium sulfate, 10 mM magnesium chloride, 10 mM manganese chloride, and 50 mM potassium 3-(N-morpholino)-propanesulfonic acid (MOPS) (pH 7.0) at 18 °C. Crystals appeared in ~1–2 weeks.

Crystals were cryoprotected in a reservoir solution containing 3.4 M ammonium sulfate, 10 mM magnesium chloride, 10 mM manganese chloride, 50 mM potassium MOPS (pH 7.0), and 15% (v/v) glycerol and then flash-frozen in liquid nitrogen. X-ray diffraction data for PSO- and PS2-SRL were collected at a wavelength of 0.9785 Å on the 21-ID-G LS-CAT beamline at the Advanced Photon Source (APS, Argonne National Laboratory, Argonne, IL), using a Mar300 CCD detector. All data were processed using HKL 2000.[41] Data for Sp-MePO-SRL were collected using the D8 Venture (Bruker AXS, Madison, WI) system in the Biomolecular Crystallography Facility in the Vanderbilt University Center for Structural Biology. The system includes an Excillum D2+ MetalJet X-ray source with Helios MX optics providing Ga Kα radiation at a wavelength of 1.3418 Å. The crystal was mounted on a kappa axis goniometer and maintained at 100 K using an Oxford Cryosystems Cryostream 800 cryostat. The detector was a PHOTON III charge-integrating pixel array detector. Data collection was performed in shutterless mode. Data were reduced using Proteum3 software (Bruker AXS). Selected crystal data and data collection statistics are summarized in Table S3.

The PSO- and PS2-SRL structures were determined by molecular replacement with MOLREP[42] using the crystal structure of the native SRL RNA as a search model (PDB entry 3DVZ).[30] In the case of the PSO-SRL(s), the values for R_{work} and R_{free} after four rounds of refinement in Refmac5[43] were 0.21 and 0.23, respectively. After the PSO moieties had been inserted, refinement was continued in Shelx[44] and groups of water molecules were gradually assigned to peaks of super-imposed Fourier $2F_o - F_c$ sum and $F_o - F_c$ difference electron densities using Coot[45] and included in the refinement. In the case of the PS2-SRL structure, it was found after five rounds of refinement in Refmac5[43] that the R factors remained relatively high ($R_{work} = 0.25$; $R_{free} = 0.32$). When the twin option was used, the values for both R-factors dropped precipitously. All further refinements were therefore carried out with the "amplitude-based twin refinement" option switch on. Diffraction data for Sp-MePO-SRL were phased using Phaser[46] and the model refined in the PHENIX suite[47] using phenix.refine.[48] The data were refined as a merohedral twin with twin law, $h, -k, -l$. Manual model fitting and visualization were performed using COOT.[45] Final refinement parameters are summarized in Table S3, and examples of the quality of the final electron density are shown in Figure S8.

Atomic coordinates and structure factors for PSO-SRL, PS2-SRL, and Sp-MePO-SRL have been deposited as PDB entries 7JJD, 7JJE, and 7JJF, respectively.

QM/MM and QM Calculations. All geometry optimization calculations for the model systems were performed at the MP2 level of theory with the aug-cc-pVDZ basis set. In the partial geometry optimization calculations, the P–O or P–S bond vector relative to the guanine base was restrained to maintain the orientation observed in the SRL crystal structures. Final energies for the geometry-optimized complexes were computed at the CCSD(T) level of theory with the aug-cc-pVDZ basis set. Local minima were confirmed via frequency calculations. All geometry optimization and energy calculations were performed with the Gaussian 16 package.[49]

Energy minimization calculations for the ACGAGAGG octamer were performed using coupled QM/MM calculations with AMBER14[50] and Gaussian 16[49] packages. The octamer fragments were extracted from the PO2- and PS2-SRL crystal structures, and both were solvated in a truncated octahedral box with a 14 Å buffer zone between any nucleotide atom and the closest box wall. Both starting complexes were subjected to a three-step minimization procedure. First, nucleotide atoms were relaxed for 10000 steps of conjugate gradient minimization while water molecules and counterions were restrained at starting positions. Next, all solvent and counterions were relaxed for 10000 steps while nucleotide atoms were restrained. Finally, all restraints were removed and the entire system was minimized for 10000 additional steps. Distance restraints were imposed to maintain the H-bonding interactions between A1 and G8 in the fragment in all minimization calculations. These limited restraints proved to be sufficient to preserve the structural integrity of this eight-nucleotide fragment during the geometry optimization calculations. The AMBER ff14 potential function[51] was used for the MM calculations (i.e., the "MM" zone) along with the SPC/E water model,[52] and Joung/Cheatham parameters were used for monovalent cations with SPC/E water.[53] The phosphate or dithiophosphate group, together with the interacting guanine base, was treated quantum mechanically (i.e., the "QM" zone). The QM zone boundaries were defined to dissect carbon–carbon and carbon–oxygen single bonds, and the linked-atom method was used to treat the QM/MM boundary. The QM zone was computed at the MP2 level of theory with a 6-311++G(2d,2p) basis set. All minimization calculations were run until the root-mean-square gradient was <0.05 kcal mol^{-1} Å^{-1}.

Graphical analyses of the complexes and figure generation were performed using UCSF Chimera.[54]

■ RESULTS

Effect of PSO and PS2 Substitutions on SRL Stability.
To examine the potential effects on the stability of a face-on
phosphate−π contact upon replacement of the PO2 by either a
PSO or PS2 moiety, we turned to the *E. coli* SRL motif. We
synthesized three 27mer RNAs, namely, the native SRL (PO2-
SRL), the SRL with a 1:1 mixture of *Rp*- and *Sp*-PSO between
A2660 and G2661 (mixed PSO-SRL), and the SRL with these
nucleosides linked by a PS2 moiety [PS2-SRL (Figure 1,
Figure S1, and Table S1)]. The *Rp*-PSO and *Sp*-PSO SRL
diastereomers were separated by RP-HPLC (Figure S1).

We used UV melting studies to determine the melting
temperatures (T_m) of the five SRLs (Figure S3). At 2 μM RNA
in 1× PBS, the T_m values of the mixed PSO-SRL (63.6 °C),
Rp-PSO SRL (64.4 °C), and PS2-SRL (63.4 °C) were
markedly higher than those of the native SRL (58.1 °C) and
the *Sp*-PSO SRL (59.1 °C) (Table 1). Thus, a single *Rp*-PSO

Table 1. SRL T_m Values and Thermodynamic Parameters

SRL	T_m (°C)	$\Delta H°$ (kcal mol^{-1})	$T\Delta S°$ (kcal mol^{-1})	$\Delta G°$ (kcal mol^{-1})
PO2	58.1 ± 0.5	−41.0 ± 1.4	−37.0 ± 1.2	−4.0 ± 0.2
PSO	63.6 ± 0.3	−57.7 ± 2.1	−51.3 ± 1.9	−6.4 ± 0.2
Rp-PSO	64.4 ± 0.6	−75.9 ± 1.2	−67.2 ± 1.0	−8.7 ± 0.2
Sp-PSO	59.1 ± 0.0	−49.9 ± 1.7	−44.9 ± 1.5	−5.0 ± 0.2
PS2	63.4 ± 0.3	−66.9 ± 1.6	−59.4 ± 1.4	−7.5 ± 0.2

modification stabilizes the SRL by 6.3 °C. We extracted
thermodynamic parameters from the monomeric SRL melting
transition curves following the protocol by Marky and
Breslauer (Figures S4−S7 and Table S2).[40] The analysis
demonstrates that the differences in free energy ($\Delta\Delta G°$)
between the PO2 and *Rp*-PSO and PO2 and PS2 SRLs are
−4.7 and −3.5 kcal mol^{-1}, respectively, whereby the enthalpy
makes the dominant contribution (Table 1). Although the
mixed PSO SRL (composed of a diastereoisomeric mixture)
and the PS2 SRL exhibit similar melting temperatures, they
differ quite significantly in terms of their thermodynamic
parameters, consistent with deviating shapes of their melting
curves (Figure S3).

**Crystal Structures of PSO- and PS2-Modified SRL-
RNAs.** The crystal structure of the native *E. coli* 23S SRL had
previously been determined at resolutions of ≤1 Å[29,30] (PDB
entry 3DVZ[30]). To visualize the modified tetraloop con-
formations, we determined the crystal structures of the PS2-
and PSO-SRLs at 1.1 and 1.15 Å resolution, respectively
(Figure S8 and Table S3). Both structures are isomorphous
with the PO2-SRL crystal structure. The root-mean-square
deviations based on overlays of all atoms among the three
SRLs are <0.1 Å. Slight differences occur in the GAGA
tetraloop region. The *Rp*- and *Sp*-PSO diastereoisomers
display slightly different conformations locally that are resolved
in the electron density map at high resolution (Figure S8a).
Moreover, in the PS2-SRL, the α, β, and γ backbone angles of
residue G2661 are all in the antiperiplanar (*ap*) conformation,
and the sugar pucker is C2′-*exo* (Figure 2). In the PO2- and
PSO-SRLs, these three backbone angles are in the standard
synclinal− (*sc*−), *ap*, and *sc*+ conformations (α to γ) and the
sugar puckers fall into the C3′-*endo* range.

Interestingly, the distances along the normal to the guanine
plane for SP2 sulfur and OP2 oxygen atoms are very similar
(Figure 2). In the case of the PO2- and *Sp*-PSO-SRLs, the
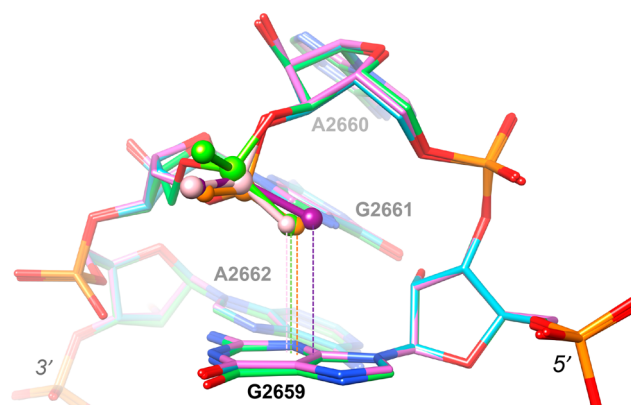
			vdW radius
PO2:	G2661-OP2 .... G2659-plane = 3.20 Å		
PS2:	G2661-SP2 .... G2659-plane = 3.27 Å	C	1.70 Å
Sp-PSO:	G2661-OP2 .... G2659-plane = 3.20 Å	S	1.80 Å
Rp-PSO:	G2661-SP2 .... G2659-plane = 3.23 Å	O	1.52 Å

Figure 2. Overlay of the tetraloops from the PO2- (PDB entry
3DVZ[30]), PS2-, and PSO-SRL crystal structures. Carbon atoms of the
three molecules are colored light blue, green, and lilac, respectively.
PO2, PS2, *Sp*-PSO, and *Rp*-PSO moieties of residue G2661 are
highlighted in ball-and-stick mode and are colored orange, light green,
pink, and purple, respectively. Vertical distances between SP2 or OP2
atoms from the phosphate, thiophosphate, and dithiophosphate
moieties and the guanine plane of residue G2659 are indicated with
thin dashed lines and are given in angstroms below the illustration,
along with the van der Waals radii of carbon, sulfur, and oxygen.

OP2-guanine distance corresponds to the sum of the van der
Waals radii of oxygen and carbon (3.22 Å), but for SP2 atoms,
the distance to guanine is well below the sum of the van Waals
radii of sulfur and carbon (3.5 Å): −0.27 Å (*Rp*-PSO SP2) and
−0.23 Å (PS2 SP2). These observations clearly argue against
the larger sulfur atom being pushed away from guanine relative
to oxygen. Rather, the tight face-on contact between the
negatively charged PS2 and *Rp*-PSO moieties and guanine is
energetically favorable as indicated by the T_m values and
thermodynamic data.

**Roles of Water and a Potential Hydrophobic Effect in
the Phosphate−Base Contact.** Inspection of the distribu-
tions of water molecules around the PO2-, PS2-, and PSO-
SRLs in the respective crystal structures shows that a majority
of the positions are maintained (Figure 3). Distances between
water molecules and sulfur atoms are as expected longer than
those between water and phosphate oxygens on average. For
phosphate oxygens, the lengths of H-bonds to waters are in the
range of 2.7−3.0 Å, and the corresponding distances involving
thiophosphate sulfurs lie between 3.1 and 3.5 Å. This was
previously seen in atomic-resolution structures of PS2-
modified RNA duplexes.[33] Considering the surroundings of
the O/SP1 and O/SP2 H-bond acceptors in the SRL loop, it is
clear that the former are more exposed to solvent molecules.
The OP2 or SP2 atoms that hover above the guanine plane of
nucleotide 2659 can establish an H-bond to only a single water
(marked by an asterisk in Figure 3). This site is indeed
occupied by a solvent molecule in the PO2-, PS2-, and PSO-
SRL crystal structures. Access for water molecules to OP2 or
SP2 atoms from the backside is blocked by the nucleobase of
G2661 and the ribose of G2659, whereby N7(2661) and
O2′(2659) are engaged in an H-bond. Overall, the SRL
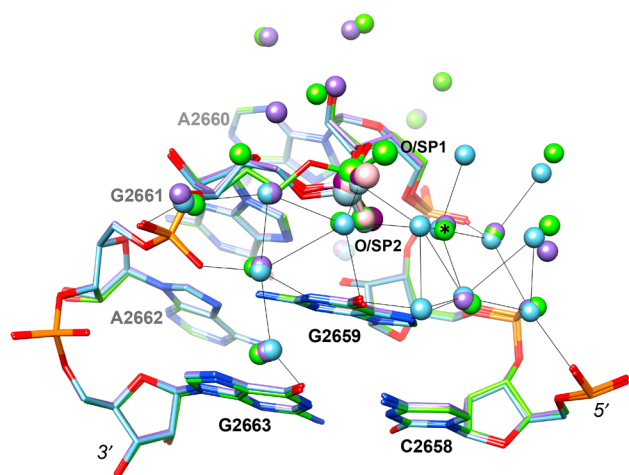structural data do not support a pivotal role of a hydrophobic

Figure 3. Distributions of water molecules around superimposed loop nucleotides of the PO2-, PS2-, and PSO-SRLs. Carbon atoms of the three RNAs are colored light blue, green, and lilac, respectively. PO2, PS2, *Sp*-PSO, and *Rp*-PSO moieties of residues G2661 are highlighted in ball-and-stick mode and are colored light blue, green, pink, and purple, respectively. Water molecules in the three SRL structures within an 8 Å radius sphere around the phosphorus atom of residue G2661 in the PO2-SRL are shown as spheres with colors matching carbon atoms. H-Bonds involving water molecules in the native SRL are drawn with thin solid lines.

effect in the increased stability of the PSO- and PS2-SRLs compared to the parent RNA folding motif.

Model System Calculations. To gain a better understanding of the individual contributions to the total interaction energies for the phosphate and dithiophosphate moieties with guanine, we turned to QM calculations. We first performed a series of full and partial geometry optimization calculations for guanine−phosphate ($G{\cdots}PO_4H_2^-$) and guanine−dithiophosphate ($G{\cdots}PO_2S_2H_2^-$) model system complexes. We do not expect that these simple model systems will represent adequately all of the key contributing energetic factors for these complexes. Ideally, we would also include the base-paired adenine (A2662) and the A2662 backbone phosphate that forms a strong H-bond with the amino group of G2659 (see Figures 1b and 2). However, a model system that includes all of these components is much too large to study at the level of theory we have used for previous calculations.[37] Even with the intrinsic limitations of our model systems, these calculations do provide some useful information. In particular, partial geometry optimization calculations in which the phosphate or dithiophosphate position relative to the guanine base was restrained at the crystallographic positions while all other degrees of freedom were relaxed reveal that the face-centered guanine−phosphate and guanine−dithiophosphate interactions observed in the crystal structures are stable local minima. Depending upon the level of QM theory and basis set used, the intrinsic phosphate−guanine interaction is roughly iso-energetic or else only slightly more stable (∼1−2 kcal mol^{-1}) than the corresponding dithiophosphate−guanine interaction. These calculations also show that the short dithiophosphate−guanine contact distances observed in the crystal structure represent an energetically stable structure, even though "chemical intuition" might suggest that such short contact distances should be strongly repulsive. Full geometry optimization for these simple model complexes yields structures where the phosphate group shifts dramatically to

form an edge-on H-bonding interaction with the guanine N1 hydrogen and amino group. In the case of the phosphate group, the interaction is similar to that observed in the tetraloop crystal structures [e.g., G2659 with the phosphate group of A2662 in PDB entry 3DVZ (Figure 2)]. The shift observed for the dithiophosphate group after full geometry optimization is less dramatic, and this complex retains some partial stacking with the base but displays no significant H-bond formation with guanine.

Given that we cannot pursue detailed QM calculations for truly relevant model systems, we next performed a series of QM/MM calculations for the eight-nucleotide ACGAGAGG fragment shown in Figure 1b that contains the GAGA tetraloop. We performed full geometry optimization for both the native and dithiophosphate-substituted loop structures. Both optimized structures display excellent agreement with the crystal structures. In particular, we observe nearly identical sulfur−guanine distances in the QM/MM calculations as reported for the X-ray structure. These results, combined with the high-level QM calculations for the guanine−phosphate/dithiophosphate complexes, strongly imply that the short sulfur−guanine contact distances are not merely a crystallographic artifact but indeed reflect a strong, favorable guanine−dithiophosphate interaction.

Previous QM and QM/MM calculations for an RNA aptamer−thrombin complex suggested that the dramatic binding affinity enhancement observed for dithiophosphate substitution at a specific RNA backbone position was due to a combination of more favorable polarization and dispersion interactions between the dithiophosphate group and a phenylalanine side chain in thrombin, compared to the corresponding interactions for the phosphate in the wild-type RNA complex.[37] It appears that the same factors can explain the unexpected RNA tetraloop stabilization we observe when a thio- or dithiophosphate group is substituted at G2661, with some caveats. The model system calculations demonstrate that greatly enhanced dispersion attraction interactions help to explain the unexpectedly short contact distances between dithiophospate and guanine in the stacked complex. While it is possible that enhanced polarization interactions in the thiophosphate- and dithiophosphate-substituted RNAs may also contribute to the enhanced stabilization, the computational results are less straightforward.

In the previous RNA aptamer−thrombin complex studies,[36] we performed single-point QM/MM energy calculations for the geometry-optimized complexes using the electrostatic embedding protocol, where the QM zone is polarized by the electric field due to all neighboring residues, solvent, and counterions in the MM zone, and then recalculated the single-point energies with the mechanical embedding protocol, which neglects the effect of the electric field produced by the point charges in the MM zone. While this is a somewhat simplistic strategy for assessing polarization contributions, it does provide a qualitative evaluation. Therefore, we used this protocol to investigate the polarization contributions in the wild-type and dithiophosphate-substituted tetraloop structures. Unlike the earlier aptamer−thrombin complex, where the dithiophosphate−phenylalanine ring interaction was effectively sequestered in a nonpolar pocket well shielded from solvent and counterions, the phosphate/dithiophosphate−guanine stacking interaction in the tetraloop is fully exposed to solvent and counterions (Figure 3). Furthermore, multimicrosecond duration classical MD simulations for the wild-type RNA

reveal that while the sodium counterions do interact strongly with the polyanion backbone, they are not completely immobilized. The dynamic fluctuations of water and counterions in the immediate vicinity of the phosphate—guanine stacking complex modulate the local electric field and lead to an apparent dampening of this field. Our analysis is based on a limited number of structural snapshots rather than a full ensemble due to the computational expense of this protocol, so we cannot draw quantitative conclusions from these calculations. However, it appears that polarization contributions may be less significant in the tetraloop stabilization observed in this study and that enhanced dispersion attraction interactions dominate.

Role of the Negative Charge of Phosphate. To explore the role of the negative charge of PO2, PSO, and PS2 moieties linking A2660 and G2661 in the SRL tetraloop in their relative stabilities (i.e., PSO-SRL ≈ PS2-SRL > PO2-SRL), we synthesized SRLs with a neutral methylphosphonate (MePO) group at that loop location. Because of the particular synthetic strategy used to generate MePO-SRLs, an additional change besides replacement of the negatively charged moiety with a neutral one concerns residue A2660 that is now a 2′-deoxyribonucleotide [dA (Table S1)]. To ascertain that replacement of the ribose at that site by a 2′-deoxyribose did not affect stability significantly, we synthesized dAPO2-, dAPSO-, and dAMePO-SRLs. T_m values and thermodynamic parameters for the dAPO2- and dAMePO-SRLs are listed in Table 2, and a full account of the experimental data for SRLs with dAPO2, dAPSO, or dAMePO moieties in the SRL loop is provided in Figures S9—S12 and Tables S4 and S5.

Table 2. T_m Values and Thermodynamic Parameters for SRLs with a PO2 or a Neutral MePO Moiety Linking dA2660 and G2661

SRL	T_m (°C)	$\Delta H°$ (kcal mol^{-1})	$T\Delta S°$ (kcal mol^{-1})	$\Delta G°$ (kcal mol^{-1})
dAPO2	59.8 ± 0.3	−48.0 ± 1.2	−43.2 ± 1.0	−4.8 ± 0.2
dAMePO	60.4 ± 0.3	−51.1 ± 2.4	−45.7 ± 2.1	−5.4 ± 0.3

As in the case of the PO2- and dAPO2-SRLs (ΔT_m = 1.7 °C), the stabilities of PSO- and dAPSO-SRLs show a high degree of similarity (Table S5). This indicates that a DNA instead of an RNA nucleotide at A2660 does not significantly affect SRL stability. Conversely, removing the negative charge on the phosphate, even when one of the nonbridging oxygens is replaced by a methyl moiety (MePO), does not boost SRL stability like in the case of the Rp-PSO and PS2 modifications. This provides further experimental support for the notion that polarization probably does not play a key role in the sulfur-mediated SRL stability increases. We were also able to separate the two MePO diastereoisomers by ion-exchange (IEX) chromatography, and RP-HPLC traces of the IEX-purified peak 1 (faster-eluting) and peak 2 (slower-eluting) MePO-SRLs are depicted in Figure S2. The melting temperatures of the two RNAs are very similar: 60.2 ± 0.3° (peak 1) and 60.6 ± 1.0° (peak 2) (Table S5). We crystallized peak 1 and determined its structure at 1.2 Å (Table S3). Accordingly, peak 1 is the Sp-MePO SRL with the methyl group hovering above the guanine plane (Figure 4). When the T_m data presented above for the two neutral MePO analogues are considered, one can conclude that a methyl or a P=O group stacked atop a guanine plane results in similar stabilities. However, the
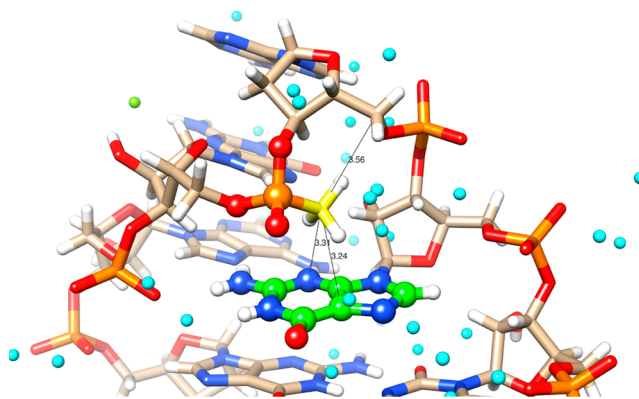

Figure 4. Close-up view of the tetraloop conformation in the Sp-MePO-SRL with the methyl group (colored yellow) stacked on top of G2659 (green carbon atoms). Water molecules are shown as cyan spheres, and distances in angstroms are drawn with thin solid lines.

proximity between a hydrophobic moiety (CH$_3$ in Sp-MePO) and the guanine π electron system is no match for the corresponding interaction involving sulfur in the Rp-PSO or PS2 systems. The vertical distance between Sp-MePO methyl carbon and guanine plane is 3.0 Å. This is very tight given that the sum of the vdW radii for the two is ca. 3.5 Å. Even if a methyl moiety stacked on guanine might be energetically favorable, the spacing in the modified SRL is too close and consistent with a repulsive interaction.

■ DISCUSSION

The QM/MM calculations for the eight-nucleotide fragment that contains the GAGA tetraloop structure are in excellent agreement with the corresponding crystal structures and suggest that the unusually short sulfur—guanine contact distances we observe are likely due to more favorable dispersion interactions between dithiophosphate and guanine compared to the native phosphate group. Unlike the earlier RNA aptamer—thrombin studies,[36,37] favorable polarization contributions for dithiophosphate substitution are not obvious in these calculations, and the experimental results for the neutral methyl phosphate substitution further support the idea that polarization does not make a major contribution to enhanced tetraloop stability. These calculations also help explain the increased thermodynamic stability of the dithiophosphate-substituted SRL relative to the wild-type molecule, which is dominated by the enthalpic component in the experimental measurements. Taken together, these two independent studies further demonstrate the significant impact that the incorporation of dithiophosphate at strategic RNA backbone positions may have on stability and/or intermolecular interactions.[33−36] By extension, the underlying reasons for the increased stability of the PS2-modified SRL also apply to the Rp-PSO SRL.

What about the possibility that nonbridging sulfurs do not directly stabilize the SRL but rather destabilize its unfolded state? Thus, tetraloops were shown to operate by unfolded state effects upon introduction of conformationally restricted nucleotides.[55−57] Moreover, loss of unsatisfied H-bonding by sulfur substitution has been shown to lead to stability without any substantial interactions in the folded state.[58] It is difficult to envision how the phosphate group of G2661 could deviate substantially from others in terms of its interactions in the unfolded state, i.e., phosphate exposed on the surface and

interacting with solvent molecules. In addition, both non-bridging phosphate oxygens are capable of forming H-bonds to solvent in the folded state (Figure 3). By contrast, there is very strong evidence from the combined stability, structural, and computational data presented here that the stacking interactions between thiophosphate and guanine on one hand and phosphate and guanine on the other differ. Thus, the distance of the OP2 phosphate oxygen and the guanine plane basically equals the sum of the van der Waals radii of carbon and oxygen. Conversely, the SP2 thiophosphate sulfur literally dives into the guanine π cloud, resulting in a vertical distance between the sulfur and guanine plane that almost matches that seen for the phosphate–guanine stacking interaction. The fact that dispersive interactions have something to do with the observed, surprisingly potent gain in stability does then not come as a surprise.

The observed stabilization afforded by mixed PSO moieties stacked on top of guanine (+5.5 °C in T_m relative to PO2) is highly unusual as this backbone modification typically results in a slight destabilization. Incorporation of a single PSO moiety into DNA and RNA decreases the T_m of a duplex by ~1 °C.[59−62] Thus, the stacking interaction involving PSO diastereoisomeric SRLs (Rp/Sp mixture) investigated here results in a dramatic gain of almost 7 °C (ΔT_m) relative to the (diastereoisomeric) modification in a canonical duplex environment. The thermodynamic analysis of the stereopure PSO-SRLs demonstrates the superior stability of the Rp-PSO isomer, with the sulfur stacked atop guanine. However, for practical purposes, a boost in stability can be achieved with the diastereoisomeric PSO mixture, thus precluding the need for potentially laborious separation or chemical synthesis. GNRA and UNR sequence motifs for use in siRNA, aptamer, ribozyme, nanotechnological, and biophysical (such as crystallization constructs) applications can be readily PSO-modified to exploit the gain in folding stability. Phosphate–base stacking has also been observed in the DNA context, e.g., between diagonal loops in the nuclear magnetic resonance solution structure of a G-quadruplex, whereby the π system is an adenine.[63]

Favorable PSO-mediated protein–DNA and –RNA interactions compared to the parent all-PO2 species are commonly attributed to diastereoisomer-specific hydrophobic contacts.[64,65] However, in this study, the key contribution to the increased stability afforded by the Rp-PSO– and PS2–base face-on interaction stems primarily from enhanced dispersion attraction, as suggested by the calculations and dramatically supported by the thermodynamic measurements for the Rp-PSO stereoisomer that forms a face-centered complex with guanine. The observed similar stabilities of the PO2– and MePO–G interactions further support the conclusion that hydrophobics cannot be the main driver for the stability increases seen with thiophosphates. Polarization dominates the dramatic increases in RNA–protein binding affinities enabled by edge-on PS2–π interactions,[36,37] while enhanced dispersion attraction explains the increased stability observed for incorporation of dithiophosphate or Rp-PSO into the SRL. Both of these examples constitute unexpected effects of thiophosphate modification that strongly benefit intra- and intermolecular stability and potentially activity, in addition to the well-documented advantage of increased nuclease stability. It is important that as far as stability gains are concerned, thioether (i.e., methionine) or sulfhydryl (i.e., cysteine)

moieties stacked on a nucleobase[25] cannot compete with the face-on thiophosphate–base interaction analyzed here.

Finally, it is noteworthy that new RNA tetraloop sequence families are still being identified. In a recent report, Znosko and colleagues classified and characterized three new clusters: U[YGAR]G, K[UGGU]M (K = G or U, and M = A or C), and Y[RMSA]R (M = A or C, and S = G or C).[66] Interestingly, two of these tetraloop families feature phosphate–nucleobase stacking. In the case of YGAR, the phosphate (OP2 oxygen) of Y stacks on G [e.g., PDB entry 5DM6, Y = U, residue 827.X (Figure 5a)]. The mode of interaction, including the oxygen–
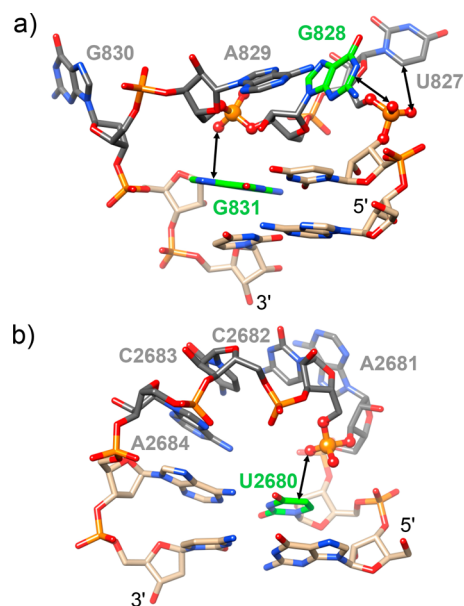

Figure 5. Phosphate–base stacking interactions in newly classified RNA tetraloop families. Carbon atoms of tetraloop residues are colored gray, and the phosphate shown in ball-and-stick mode stacks on the green base. (a) YGAR≡UGAG. In addition to the phosphate of U827 stacking on G828, the same phosphate also engages in an edge-on intraresidue contact with uracil C5 (4.1 Å) and the phosphate of A829 stacks on G831 (arrows). (b) RMSA≡ACCA. The phosphate of C2682 stacks on U2680 (arrow).

guanine distance, is very similar to the situation in the SRL GAGA tetraloop. In the Y[RMSA]R family, the phosphate (OP2 oxygen) of M stacks on the nucleobase of Y [e.g., PDB entry 5DM7, Y = U, M = C, residue 2682.X (Figure 5b)]. Here the nucleobase is uracil as in the case of the U-turn. These examples demonstrate that the commonly ignored phosphate–nucleobase stacking interaction is perhaps more common than previously assumed.

Our analysis shows that a well-established chemical modification of the phosphate moiety stabilizes the stacking interaction to a significant degree. The gain is enthalpic in nature, with a dominant contribution from dispersion attraction. Thus, this somewhat unusual environment of an RNA backbone phosphate group has revealed a new and unexpected behavior of the arguably old and well-studied thiophosphate modification.

■ CONCLUSIONS

Tetraloops and the ribosomal sarcin/ricin loop (SRL) have been the focus of numerous investigations regarding RNA structure and function. Replacement of a nonbridging

phosphate oxygen by sulfur in DNA and RNA (PSO, phosphorothioate) represents one of the earliest[67] and most common modifications in nucleic acid therapeutics.[62] Remarkably, *R*p-PSO modifications are widespread in the DNA of prokaryotes, including human pathogens and may serve a protective role against nucleases.[68] Loss of PSO modification as a result of oxidative stress causes genomic instability.[69] Recently, it was shown the *R*p-PSO modification also occurs in rRNA of prokaryotes and eukaryotes.[70] GNRA and many other classes of tetraloops have been analyzed in solution and in crystals, and the sequence dependence of their stability and conformational characteristics have been studied in detail. Not surprisingly, as far as descriptions of the conformation of tetraloops are concerned, the emphasis is on base stacking, H-bonding, and the role of observed solvent molecules and/or metal ions. However, a conserved and unusual feature of GNRA tetraloops, namely a phosphate group stacked onto the nucleobase of the first residue (G), is always ignored. We wondered whether this marriage between a negative charge and a π system is merely tolerated or actually makes a stabilizing contribution, the latter possibility potentially explaining its conservation in the folding motif. We probed the stacking interaction with the PSO and PS2 modifications and found that both stabilize the SRL to a significant degree relative to the parent loop with a PO2 moiety (Figure 6), with the *R*p-PSO SRL exhibiting the highest stability. The gain is enthalpic in nature, with a dominant contribution from

dispersion attraction. By comparison, replacing the negatively charged phosphate with a neutral methylphosphonate moiety [MePO (Figure 6)] is less remarkable in terms of SRL stability. This observation argues against a crucial role of charge in the native loop and a favorable contribution to stability beyond that afforded by the oxygen–guanine lp–π interaction.

The common answer to the question of what happens if a (negatively charged) oxygen engaged in a face-on interaction with an aromatic moiety in a tight RNA turn is replaced with a larger sulfur would likely be "a steric conflict". We demonstrate here not only that this is not the case but also that PSO/PS2 modification results in an unexpectedly large stabilization. Thus, our work at the intersections of RNA structure, function, and modification offers surprising insights from basic science into the contrasting behavior of two neighbors in the periodic table and fundamental properties of RNA folding stability and conformation. Neither the regiospecific stabilization of the SRL GAGA tetraloop caused by *R*p-PSO and PS2 modification and grounded in enhanced dispersive interactions nor the dramatically enhanced binding affinity of an RNA aptamer–thrombin complex as a result of a regiospecific PS2 modification[36] and found to be fueled by sulfur polarization[37] can be rationalized with a hydrophobic effect. These examples show that the consequences of sulfur modification in the backbone of RNA for folding stability and protein interactions are likely more nuanced than hitherto anticipated and may hold more surprises in terms of both the magnitude of the effect and its precise origin.
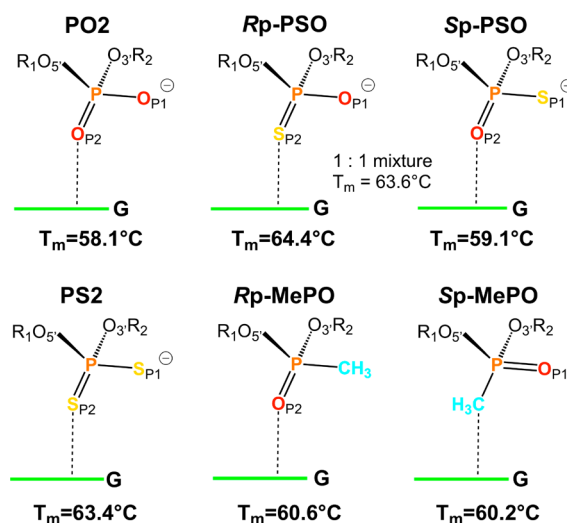
■ ASSOCIATED CONTENT

ⓈⒾ Supporting Information

The Supporting Information is available free of charge at https://pubs.acs.org/doi/10.1021/acs.biochem.0c00685.

>Oligo MS data, HPLC traces for the separation of the *R*p- and *S*p-PSO- and MePO-SRLs, UV melting curves, extraction of thermodynamic data, selected crystal data, and data collection and refinement parameters as well as quality of the final electron densities listed in Tables S1–S5 and illustrated in Figures S1–S12 (PDF)

■ AUTHOR INFORMATION

Corresponding Author

Martin Egli – *Department of Biochemistry and Center for Structural Biology, Vanderbilt University, Nashville, Tennessee 37235, United States;* ⓞ orcid.org/0000-0003-4145-356X; Phone: (615) 343-8070; Email: martin.egli@vanderbilt.edu

Authors

Pradeep S. Pallan – *Department of Biochemistry, Vanderbilt University, Nashville, Tennessee 37235, United States*

Terry P. Lybrand – *Department of Chemistry, Department of Pharmacology, and Center for Structural Biology, Vanderbilt University, Nashville, Tennessee 37235, United States;* ⓞ orcid.org/0000-0002-2248-104X

Mark K. Schlegel – *Alnylam Pharmaceuticals, Cambridge, Massachusetts 02142, United States;* ⓞ orcid.org/0000-0002-0127-608X

Joel M. Harp – *Department of Biochemistry and Center for Structural Biology, Vanderbilt University, Nashville, Tennessee 37235, United States*

Figure 6. Relative thermal stabilities of 27mer SRL-RNA and analogues with a phosphate (p) modification in the G̲ApGA tetraloop, whereby the phosphate engages in a stacking interaction with guanine (underlined). The illustrations simply indicate that phosphates and thiophosphates carry a formal negative charge while the methylphosphonates are neutral. Thus, we are not implying that more charge is localized on one atom versus another. In fact, evidence was presented many years ago that the negative charge in phosphorothioates is located on the sulfur.[71] The charge distribution can vary as a result of metal ion coordination and shift from oxygen in the presence of Mg^{2+} to sulfur in the presence of Cd^{2+}.[62,71] This difference in charge distribution as a result of the PSO interaction with hard and soft metal ions is the basis for the metal ion rescue approach in investigations of RNA folding and metal ion coordination.[72] However, the precise charge distributions between non-bridging atoms of PO2, PSO and PS2 moieties stacked on top of a nucleobase are currently not known and will be the subject of further investigations.

Hartmut Jahns − *Alnylam Pharmaceuticals, Cambridge, Massachusetts 02142, United States*

Muthiah Manoharan − *Alnylam Pharmaceuticals, Cambridge, Massachusetts 02142, United States;* ⓞ orcid.org/0000-0002-7931-1172

Complete contact information is available at:
https://pubs.acs.org/10.1021/acs.biochem.0c00685

■ DEDICATION

Dedicated to Richard Neil Armstrong (1948−2015), Professor of Biochemistry and Chemistry, Vanderbilt University. Editor-in-chief, *Biochemistry* 2004−2015.

■ ABBREVIATIONS

PDB, Protein Data Bank; PO2, phosphate; PSO, mono-thiophosphate; PS2, dithiophosphate.

■ REFERENCES

(1) Batey, R. T., Rambo, R. P., and Doudna, J. A. (1999) Tertiary motifs in RNA structure and folding. *Angew. Chem., Int. Ed. 38*, 2326−2343.

(2) Battle, D. J., and Doudna, J. A. (2002) Specificity of RNA-RNA helix recognition. *Proc. Natl. Acad. Sci. U. S. A. 99*, 11676−11681.

(3) Hendrix, D. E., Brenner, S. E., and Holbrook, S. R. (2005) RNA structural motifs: building blocks of a modular biomolecule. *Q. Rev. Biophys. 38*, 221−243.

(4) Chen, S. J. (2008) RNA folding: conformational statistics, folding kinetics, and ion electrostatics. *Annu. Rev. Biophys. 37*, 197−214.

(5) Bashan, A., and Yonath, A. (2011) Ribosome crystallography: from early evolution to contemporary medical insights. In *Ribosomes. Structure, Function and Dynamics* (Rodnina, M. V., Wintermeyer, W., and Green, R., Eds.) pp 3−18, Springer, New York.

(6) Miao, Z., and Westhof, E. (2017) RNA structure: advances and assessment of 3D structure prediction. *Annu. Rev. Biophys. 46*, 483−503.

(7) Quigley, G. J., and Rich, A. (1976) Structural domains of transfer RNA molecules. *Science 194*, 796−806.

(8) Cate, J. H., Gooding, A. R., Podell, E., Zhou, K., Golden, B. L., Kundrot, C. E., Cech, T. R., and Doudna, J. A. (1996) Crystal structure of a group I ribozyme domain: principles of RNA packing. *Science 273*, 1678−1685.

(9) Berger, I., and Egli, M. (1997) The role of backbone oxygen atoms in the organization of nucleic acid tertiary structure: zippers, networks, clamps, and C-H···O hydrogen bonds. *Chem. - Eur. J. 3*, 1400−1404.

(10) Tamura, M., and Holbrook, S. R. (2002) Sequence and structural conservation in RNA ribose zippers. *J. Mol. Biol. 320*, 455−474.

(11) Cate, J. H., and Doudna, J. A. (1996) Metal-binding sites in the major groove of a large ribozyme domain. *Structure 4*, 1221−1229.

(12) Pyle, A. M. (2002) Metal ions in the structure and function of RNA. *JBIC, J. Biol. Inorg. Chem. 7*, 679−690.

(13) Egli, M., Minasov, G., Su, L., and Rich, A. (2002) Metal ions and flexibility in a viral RNA pseudoknot at atomic resolution. *Proc. Natl. Acad. Sci. U. S. A. 99*, 4302−4307.

(14) Draper, D. E. (2004) A guide to ions and RNA structure. *RNA 10*, 335−343.

(15) Forconi, M., and Herschlag, D. (2009) Metal ion-based RNA cleavage as a structural probe. *Methods Enzymol. 468*, 91−106.

(16) Altona, C., and Sundaralingam, M. (1972) Conformational analysis of the sugar ring in nucleosides and nucleotides. New description using the concept of pseudorotation. *J. Am. Chem. Soc. 94*, 8205−8212.

(17) Thibaudeau, C., and Chattopadhyaya, J. (1999) *Stereoelectronic Effects in Nucleosides and Nucleotides and Their Structural Implications*, Uppsala University Press, Uppsala, Sweden.

(18) Rich, A. (2003) The double helix: a tale of two puckers. *Nat. Struct. Mol. Biol. 10*, 247−249.

(19) Anosova, I., Kowal, E. A., Dunn, M. R., Chaput, J. C., van Horn, W. D., and Egli, M. (2016) The structural diversity of artificial genetic polymers. *Nucleic Acids Res. 44*, 1007−1021.

(20) Egli, M. (2018) Sugar pucker and nucleic acid structure. In *The Excitement of Discovery: A Tribute to Alexander Rich* (Zhang, S., Ed.) Series in Structural Biology, Vol. *11*, pp 309−315, World Scientific Publishers.

(21) Denning, E. J., and MacKerell, A. D., Jr. (2012) Intrinsic contribution of the 2′-hydroxyl to RNA conformational heterogeneity. *J. Am. Chem. Soc. 134*, 2800−2806.

(22) Egli, M., and Gessner, R. V. (1995) Stereoelectronic effects of deoxyribose O4′ on DNA conformation. *Proc. Natl. Acad. Sci. U. S. A. 92*, 180−185.

(23) Chawla, M., Chermak, E., Zhang, Q., Bujnicki, J. M., Oliva, R., and Cavallo, L. (2017) Occurrence and stability of lone pair- stacking interactions between ribose and nucleobases in functional RNAs. *Nucleic Acids Res. 45*, 11019−11032.

(24) Egli, M., and Sarkhel, S. (2007) Lone pair-aromatic interactions: to stabilize or not to stabilize. *Acc. Chem. Res. 40*, 197−205.

(25) Egli, M. (2009) On stacking. In *Structure and Function* (Comba, P., Ed.) pp 177−196, Springer, Heidelberg, Germany.

(26) Heus, H. A., and Pardi, A. (1991) Structural features that give rise to the unusual stability of RNA hairpins containing GNRA loops. *Science 253*, 191−194.

(27) Jucker, F. M., and Pardi, A. (1995) GNRA tetraloops make a U-turn. *RNA 1*, 219−222.

(28) Correll, C. C., Munishkin, A., Chan, Y.-L., Ren, Z., Wool, I. G., and Steitz, T. A. (1998) Crystal structure of the ribosomal RNA domain essential for binding elongation factors. *Proc. Natl. Acad. Sci. U. S. A. 95*, 13436−13441.

(29) Correll, C. C., Wool, I. G., and Munishkin, A. (1999) The two faces of the Escherichia coli 23 S rRNA sarcin/ricin domain: the structure at 1.11 A resolution. *J. Mol. Biol. 292*, 275−287.

(30) Olieric, V., Rieder, U., Lang, K., Serganov, A., Schulze-Briese, C., Micura, R., Dumas, P., and Ennifar, E. (2009) A fast selenium derivatization strategy for crystallization and phasing of RNA structures. *RNA 15*, 707−715.

(31) Glück, A., Endo, Y., and Wool, I. G. (1994) The ribosomal RNA identity elements for ricin and for α-sarcin: mutations in the putative CG pair that closes a GAGA tetraloop. *Nucleic Acids Res. 22*, 321−324.

(32) Shi, X., Khade, P. K., Sanbonmatsu, K. Y., and Joseph, S. (2012) Functional role of the sarcin-ricin loop of the 23S rRNA in the elongation cycle of protein synthesis. *J. Mol. Biol. 419*, 125−138.

(33) Wu, S. Y., Yang, X., Gharpure, K. M., Hatakeyama, H., Egli, M., McGuire, M. H., Nagaraja, A. S., Miyake, T. M., Rupaimoole, R., Pecot, C. V., Taylor, M., Pradeep, S., Sierant, M., Rodriguez-Aguayo, C., Choi, H. J., Previs, R. A., Armaiz-Pena, G. N., Huang, L., Martinez, C., Hassell, T., Ivan, C., Sehgal, V., Singhania, R., Han, H. D., Su, C., Kim, J. H., Dalton, H. J., Kovvali, C., Keyomarsi, K., McMillan, N. A. J., Overwijk, W. W., Liu, J., Lee, J. S., Baggerly, K. A., Lopez-Berestein, G., Ram, P. T., Nawrot, B., and Sood, A. K. (2014) 2.-OMe-

Phosphorodithioate-modified siRNAs show increased loading into the RISC complex and enhanced anti-tumour activity. *Nat. Commun. 5*, 3459.

(34) Pallan, P. S., Yang, X., Sierant, M., Dinuka Abeydeera, N., Hassell, T., Martinez, C., Janicka, M., Nawrot, B., and Egli, M. (2014) Crystal structure, stability and Ago2 affinity of phosphorodithioate-modified RNAs. *RSC Adv. 4*, 64901–64904.

(35) Yang, X., Dinuka Abeydeera, N., Liu, F.-W., and Egli, M. (2017) Origins of the enhanced affinity of RNA–protein interactions triggered by RNA phosphorodithioate backbone modification. *Chem. Commun. 53*, 10508–10511.

(36) Abeydeera, N. D., Egli, M., Cox, N., Mercier, K., Conde, J. N., Pallan, P. S., Mizurini, D. M., Sierant, M., Hibti, F.-E., Hassell, T., Wang, T., Liu, F.-W., Liu, H.-M., Martinez, C., Sood, A. K., Lybrand, T. P., Frydman, C., Monteiro, R. Q., Gomer, R. H., Nawrot, B., and Yang, X. (2016) Evoking picomolar binding in RNA by a single phosphorodithioate linkage. *Nucleic Acids Res. 44*, 8052–8064.

(37) Egli, M., and Lybrand, T. P. (2019) Enhanced dispersion and polarization interactions achieved through dithiophosphate group incorporation yield a dramatic binding affinity increase for an aptamer-thrombin complex. *J. Am. Chem. Soc. 141*, 4445–4452.

(38) Flür, S., and Micura, R. (2016) Chemical synthesis of RNA with site-specific methylphosphonate modifications. *Methods 107*, 79–88.

(39) Frederiksen, J. K., and Piccirilli, J. A. (2009) Separation of RNA phosphorothioate oligonucleotides by HPLC. *Methods Enzymol. 468*, 289–309.

(40) Marky, L. A., and Breslauer, K. J. (1987) Calculating thermodynamic data for transitions of any molecularity from equilibrium melting curves. *Biopolymers 26*, 1601–1620.

(41) Otwinowski, Z., and Minor, W. (1997) Processing of X-ray diffraction data collected in oscillation mode. *Methods Enzymol. 276*, 307–326.

(42) Vagin, A., and Teplyakov, A. (2010) Molecular replacement with MOLREP. *Acta Crystallogr., Sect. D: Biol. Crystallogr. 66*, 22–25.

(43) Murshudov, G. N., Skubak, P., Lebedev, A. A., Pannu, N. S., Steiner, R. A., Nicholls, R. A., Winn, M. D., Long, F., and Vagin, A. A. (2011) REFMAC5 for the refinement of macromolecular crystal structures. *Acta Crystallogr., Sect. D: Biol. Crystallogr. 67*, 355–367.

(44) Sheldrick, G. M., and Schneider, T. R. (1997) SHELXL: high resolution refinement. *Methods Enzymol. 277*, 319–343.

(45) Emsley, P., Lohkamp, B., Scott, W. G., and Cowtan, K. (2010) Features and development of Coot. *Acta Crystallogr., Sect. D: Biol. Crystallogr. 66*, 486–501.

(46) McCoy, A. J., Grosse-Kunstleve, R. W., Adams, P. D., Winn, M. D., Storoni, L. C., and Read, R. J. (2007) Phaser crystallographic software. *J. Appl. Crystallogr. 40*, 658–674.

(47) Liebschner, D., Afonine, P. V., Baker, M. L., Bunkóczi, G., Chen, V. B., Croll, T. I., Hintze, B., Hung, L. W., Jain, S., McCoy, A. J., Moriarty, N. W., Oeffner, R. D., Poon, B. K., Prisant, M. G., Read, R. J., Richardson, J. S., Richardson, D. C., Sammito, M. D., Sobolev, O. V., Stockwell, D. H., Terwilliger, T. C., Urzhumtsev, A. G., Videau, L. L., Williams, C. J., and Adams, P. D. (2019) Macromolecular structure determination using X-rays, neutrons and electrons: recent developments in Phenix. *Acta Cryst. D 75*, 861–877.

(48) Afonine, P. V., Grosse-Kunstleve, R. W., Echols, N., Headd, J. J., Moriarty, N. W., Mustyakimov, M., Terwilliger, T. C., Urzhumtsev, A., Zwart, P. H., and Adams, P. D. (2012) Towards automated crystallographic structure refinement with phenix. refine. *Acta Crystallogr., Sect. D: Biol. Crystallogr. 68*, 352–367.

(49) Frisch, M. J., Trucks, G. W., Schlegel, H. B., Scuseria, G. E., Robb, M. A., Cheeseman, J. R., Scalmani, G., Barone, V., Petersson, G. A., Nakatsuji, H., Li, X., Caricato, M., Marenich, A., Bloino, J., Janesko, B. G., Gomperts, R., Mennucci, B., Hratchian, H. P., Ortiz, J. V., Izmaylov, A. F., Sonnenberg, J. L., Williams-Young, D., Ding, F., Lipparini, F., Egidi, F., Goings, J., Peng, B., Petrone, A., Henderson, T., Ranasinghe, D., Zakrzewski, V. G., Gao, J., Rega, N., Zheng, G., Liang, W., Hada, M., Ehara, M., Toyota, K., Fukuda, R., Hasegawa, J., Ishida, M., Nakajima, T., Honda, Y., Kitao, O., Nakai, H., Vreven, T.,

Throssell, K., Montgomery, J. A., Jr., Peralta, J. E., Ogliaro, F., Bearpark, M. J., Heyd, J. J., Brothers, E. N., Kudin, K. N., Staroverov, V. N., Keith, T. A., Kobayashi, R., Normand, J., Raghavachari, K., Rendell, A. P., Burant, J. C., Iyengar, S. S., Tomasi, J., Cossi, M., Millam, J. M., Klene, M., Adamo, C., Cammi, R., Ochterski, J. W., Martin, R. L., Morokuma, K., Farkas, O., Foresman, J. B., and Fox, D. J. (2016) *Gaussian 16*, rev. B.01, Gaussian, Inc., Wallingford, CT.

(50) Case, D. A., Babin, V., Berryman, J. T., Betz, R. M., Cai, Q., Cerutti, D. S., Cheatham, T. E., III, Darden, T. A., Duke, R. E., Gohlke, H., Goetz, A. W., Gusarov, S., Homeyer, N., Janowski, P., Kaus, J., Kolossváry, I., Kovalenko, A., Lee, T. S., LeGrand, S., Luchko, T., Luo, R., Madej, B., Merz, K. M., Paesani, F., Roe, D. R., Roitberg, A., Sagui, C., Salomon-Ferrer, R., Seabra, G., Simmerling, C. L., Smith, W., Swails, J., Walker, R. C., Wang, J., Wolf, R. M., Wu, X., and Kollman, P. A. (2014) *AMBER14*, University of California, San Francisco, San Francisco.

(51) Maier, J. A., Martinez, C., Kasavajhala, K., Wickstrom, L., Hauser, K. E., and Simmerling, C. (2015) ff14SB: Improving the accuracy of protein side chain and backbone parameters from ff99SB. *J. Chem. Theory Comput. 11*, 3696–3713.

(52) Berendsen, H. J. C., Grigera, J. R., and Straatsma, T. P. (1987) The missing term in effective pair potentials. *J. Phys. Chem. 91*, 6269–6271.

(53) Joung, I. S., and Cheatham, T. E., III (2008) Determination of alkali and halide monovalent ion parameters for use in explicitly solvated biomolecular simulations. *J. Phys. Chem. B 112*, 9020–9041.

(54) Pettersen, E. F., Goddard, T. D., Huang, C. C., Couch, G. S., Greenblatt, D. M., Meng, E. C., and Ferrin, T. E. (2004) UCSF Chimera − a visualization system for exploratory research and analysis. *J. Comput. Chem. 25*, 1605–1612.

(55) Ma, H., Proctor, D. J., Kierzek, E., Kierzek, R., Bevilacqua, P. C., and Gruebele, M. (2006) Exploring the energy landscape of a small RNA hairpin. *J. Am. Chem. Soc. 128*, 1523–1530.

(56) Proctor, D. J., Kierzek, E., Kierzek, R., and Bevilacqua, P. C. (2003) Restricting the conformational heterogeneity of RNA by specific incorporation of 8-bromoguanosine. *J. Am. Chem. Soc. 125*, 2390–2391.

(57) Proctor, D. J., Ma, H., Kierzek, E., Kierzek, R., Gruebele, M., and Bevilacqua, P. C. (2004) Folding thermodynamics and kinetics of YNMG RNA hairpins: specific incorporation of 8-bromoguanosine leads to stabilization by enhancement of the folding rate. *Biochemistry 43*, 14004–14014.

(58) Siegfried, N. A., Kierzek, R., and Bevilacqua, P. C. (2010) Role of unsatisfied hydrogen bond acceptors in RNA energetics and specificity. *J. Am. Chem. Soc. 132*, 5342–5344.

(59) Stein, C. A., Subasinghe, C., Shinozuka, K., and Cohen, J. S. (1988) Physicochemical properties of phosphorothioate oligodeoxynucleotides. *Nucleic Acids Res. 16*, 3209–3221.

(60) Boczkowska, M., Guga, P., and Stec, W. J. (2002) Stereodefined phosphorothioate analogues of DNA: relative thermodynamic stability of the model PS-DNA/DNA and PS-DNA/RNA complexes. *Biochemistry 41*, 12483–12487.

(61) Wan, W. B., Migawa, M. T., Vasquez, G., Murray, H. M., Nichols, J. G., Gaus, H., Berdeja, A., Lee, S., Hart, C. E., Lima, W. F., Swayze, E. E., and Seth, P. P. (2014) Synthesis, biophysical properties and biological activity of second generation antisense oligonucleotides containing chiral phosphorothioate linkages. *Nucleic Acids Res. 42*, 13456–13468.

(62) Eckstein, F. (2014) Phosphorothioates, essential components of therapeutic oligonucleotides. *Nucleic Acid Ther. 24*, 374–387.

(63) Kuryavyi, V., Majumdar, A., Shallop, A., Chernichenko, N., Skripkin, E., Jones, R., and Patel, D. J. (2001) A double chain reversal loop and two diagonal loops define the architecture of a unimolecular DNA quadruplex containing a pair of stacked G(syn)-G(syn)-G(anti)-G(anti) tetrads flanked by a G-(T-T) Triad and a T-T-T triple. *J. Mol. Biol. 310*, 181–194.

(64) Yamasaki, K., Akutsu, Y., Yamasaki, T., Miyagishi, M., and Kubota, T. (2020) Enhanced affinity of racemic phosphorothioate DNA with transcription factor SATB1 arising from diastereomer-

specific hydrogen bonds and hydrophobic contacts. *Nucleic Acids Res.* 48, 4551−4561.

(65) Hyjek-Składanowska, M., Vickers, T. A., Napiórkowska, A., Anderson, B., Tanowitz, M., Crooke, S. T., Liang, X., Seth, P. P., and Nowotny, M. (2020) Origins of the increased affinity of phosphorothioate-modified therapeutic nucleic acids for proteins. *J. Am. Chem. Soc.* 142, 7456−7468.

(66) Richardson, K. E., Adams, M. S., Kirkpatrick, C. C., Gohara, D. W., and Znosko, B. M. (2019) Identification and characterization of new RNA tetraloop sequence families. *Biochemistry* 58, 4809−4820.

(67) Eckstein, F. (1966) Nucleoside phosphorothioates. *J. Am. Chem. Soc.* 88, 4292−4294.

(68) Wang, L., Chen, S., Xu, T., Taghizadeh, K., Wishnok, J. S., Zhou, X., You, D., Deng, Z., and Dedon, P. C. (2007) Phosphorothioation of DNA in bacteria by *dnd* genes. *Nat. Chem. Biol.* 3, 709−710.

(69) Kellner, S., DeMott, M. S., Cheng, C. P., Russell, B. S., Cao, B., You, D., and Dedon, P. C. (2017) Oxidation of phosphorothioate DNA modifications leads to lethal genomic instability. *Nat. Chem. Biol.* 13, 888−894.

(70) Wu, Y., Tang, Y., Dong, X., Zheng, Y. Y., Haruehanroengra, P., Mao, S., Lin, Q., and Sheng, J. (2020) RNA phosphorothioate modification in prokaryotes and eukaryotes. *ACS Chem. Biol.* 15, 1301−1305.

(71) Iyengar, R., Eckstein, F., and Frey, P. A. (1984) Phosphorus-oxygen bond order in adenosine 5-O-phosphorothioate dianion. *J. Am. Chem. Soc.* 106, 8309−8310.

(72) Frederiksen, J. K., Li, N.-S., Das, R., Herschlag, D., and Piccirilli, J. A. (2012) Metal-ion rescue revisited: Biochemical detection of site-bound metal ions important for RNA folding. *RNA* 18, 1123−1141.

Supporting Information

Incorporating a Thiophosphate Modification into a Common RNA Tetraloop Motif Causes an Unanticipated Stability Boost

Pradeep S. Pallan[§], Terry P. Lybrand[¶,†,‡], Mark K. Schlegel[#], Joel M. Harp[§,‡], Hartmut Jahns[#], Muthiah Manoharan[#] and Martin Egli[*,§,‡]

[§]Department of Biochemistry, [¶]Department of Chemistry, [†]Department of Pharmacology, [‡]Center for Structural Biology, Vanderbilt University, Nashville, Tennessee 37235, United States, and [#]Alnylam Pharmaceuticals, 300 Third Street, Cambridge, Massachusetts 02142, United States

Contents

1. Oligonucleotide synthesis and characterization

Table S1. Analytical data for modified oligonucleotides.

Oligo	Sequence (5'->3')	Mol. Weight (Calc.)	Mol. Weight (Obs.)
PO2-SRL	UGCUCCUAGUACGAGAGGACCGGAGUG	8727.3	8725.9
PSO-SRL	UGCUCCUAGUACGA•GAGGACCGGAGUG	8743.4	8741.5
PS2-SRL	UGCUCCUAGUACGA■GAGGACCGGAGUG	8759.4	8757.4
dAPO2-SRL	UGCUCCUAGUACGaGAGGACCGGAGUG	8711.3	8710.7
dAPSO-SRL	UGCUCCUAGUACGa•GAGGACCGGAGUG	8727.4	8726.7
dAMePO-SRL	UGCUCCUAGUACGa♦GAGGACCGGAGUG	8709.3	8708.3

Uppercase and lowercase letters correspond to RNA and DNA nucleotides, respectively. PS, PS2, and MePO linkages are indicated by •, ■, and ♦, respectively.

Figure S1. Analytical RP-HPLC traces of IEX-purified mixture of PSO-SRL diastereomers (top), isolated faster eluting peak (middle, Rp diastereomer), and isolated slower eluting peak (bottom, Sp diastereomer). Samples were injected onto a Waters Xterra MS C18 column (4.6 x 100 mm, 5 µm particle size) at a flow rate of 1 mL/min and a temperature of 25 °C and eluted using a linear gradient of 6-9.5% acetonitrile in 50 mM triethylammonium acetate (TEAA) over 25 minutes.
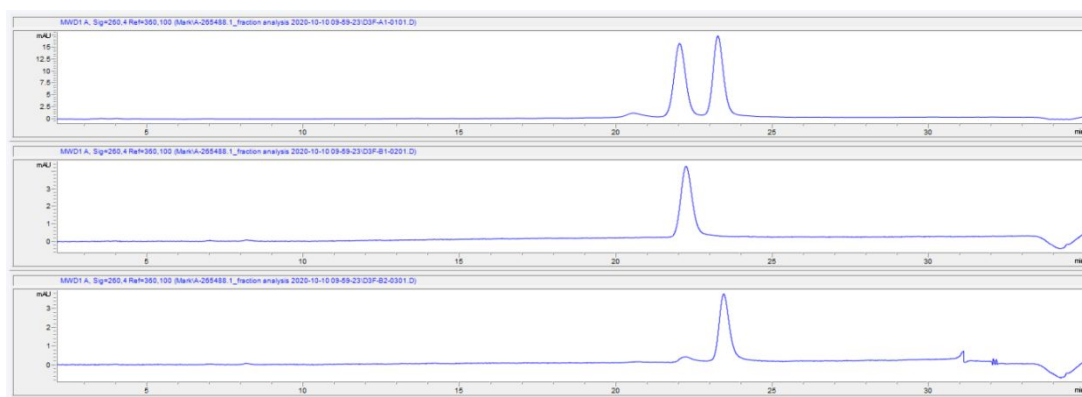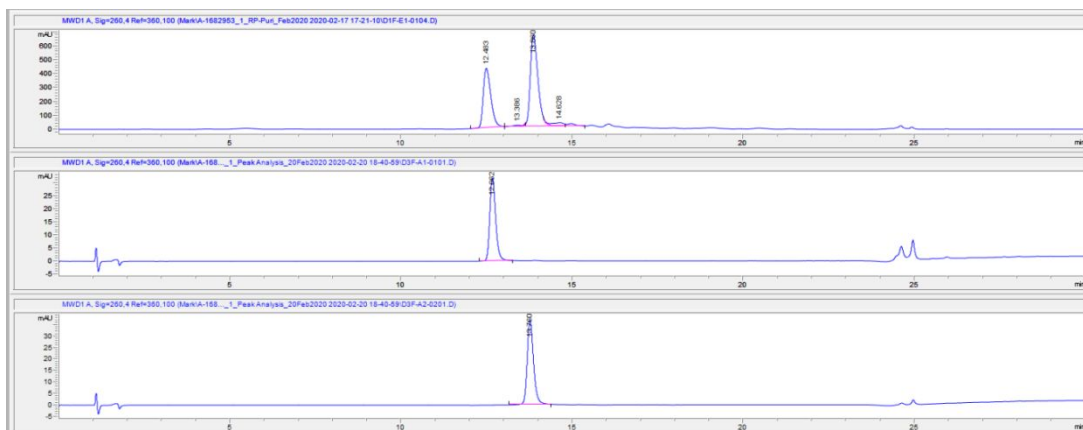
Figure S2. Analytical RP-HPLC traces of IEX-purified mixture of dAMePO-SRL diastereomers (top), isolated faster eluting peak (middle, *S*p diastereomer), and isolated slower eluting peak (bottom, *R*p diastereomer). Samples were injected onto a Waters Xterra MS C18 column (4.6 x 100 mm, 5 μm particle size) at a flow rate of 1 mL/min and a temperature of 45 °C and eluted using a linear gradient of 3-5% acetonitrile in 100 mM NH$_4$OAc over 15 minutes.
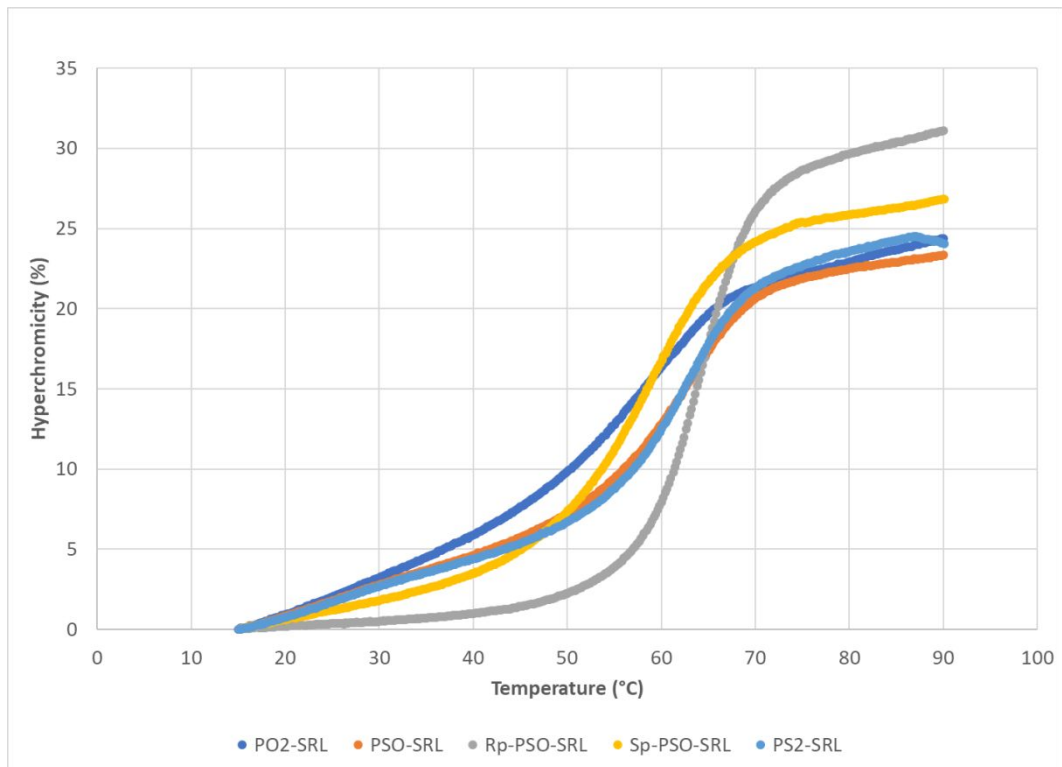
2. UV thermal melting experiments

Figure S3. Melting curves for PO2 (blue), PSO (orange), *R*p-PSO (gray), *S*p-PSO (yellow) and PS2 (light blue) SRL RNAs.
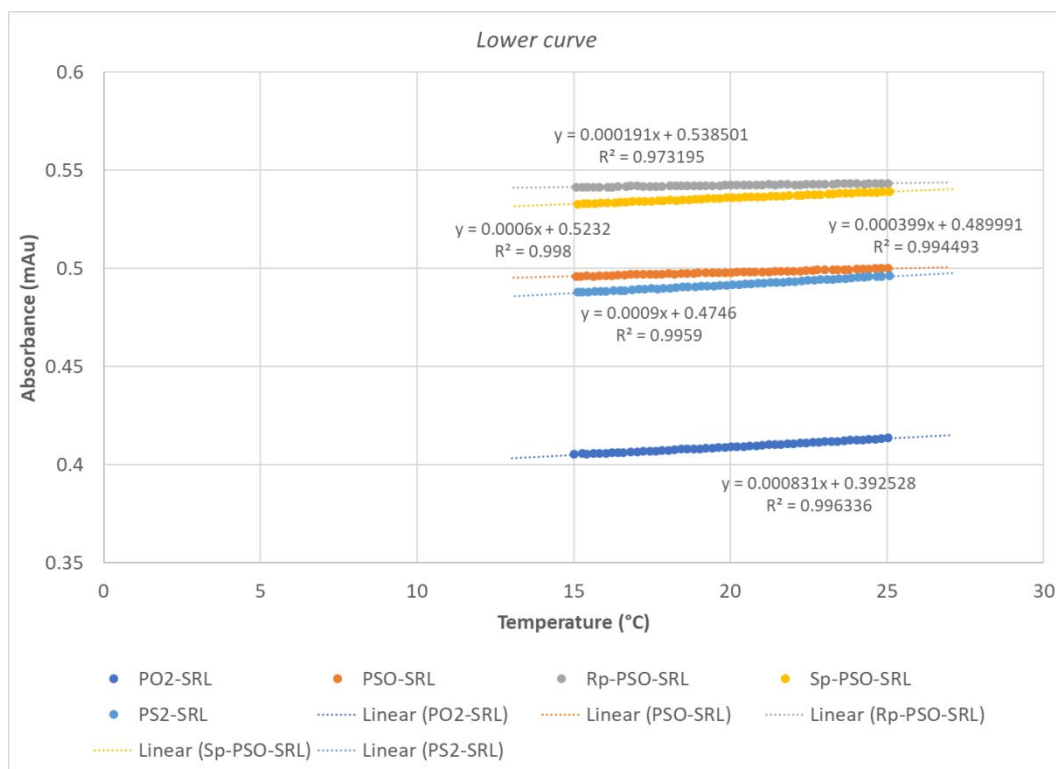
3. Calculation of thermodynamic parameters
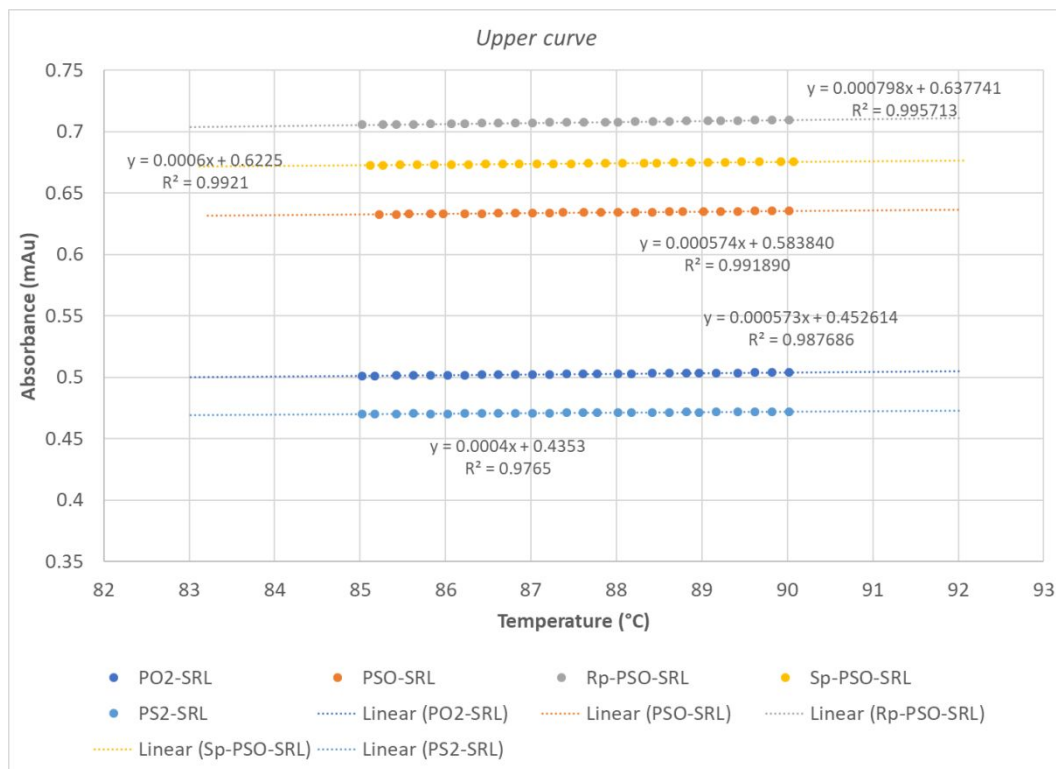

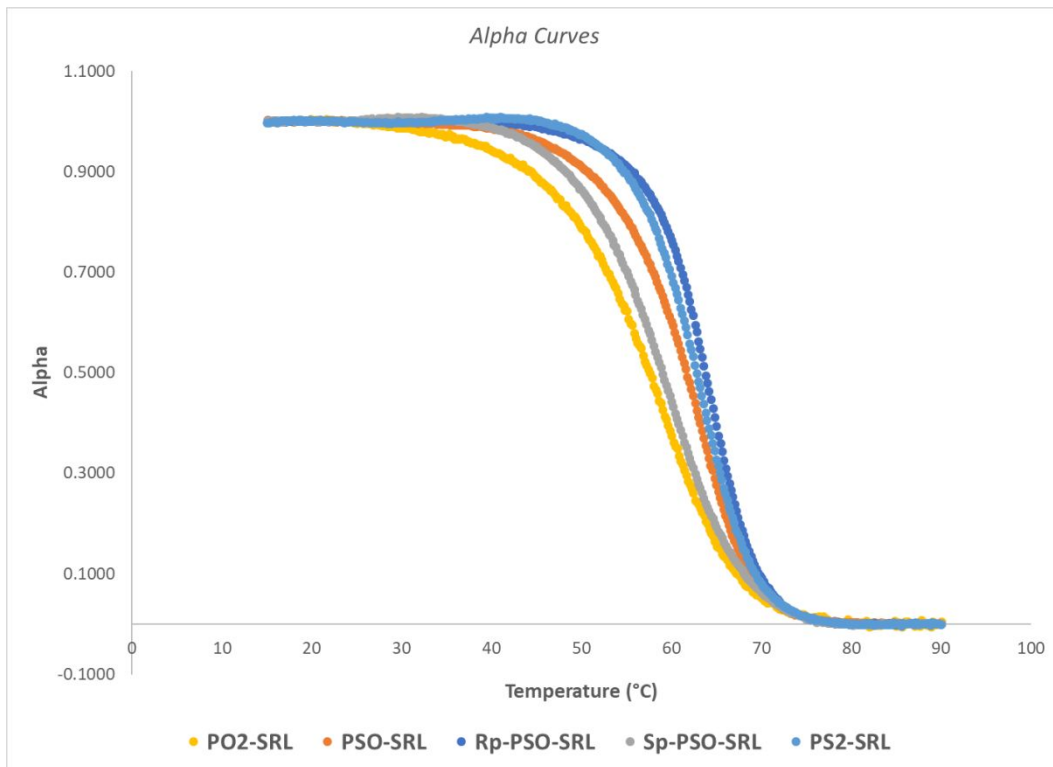**Figure S4.** Lower baselines.

Figure S5. Upper baselines.

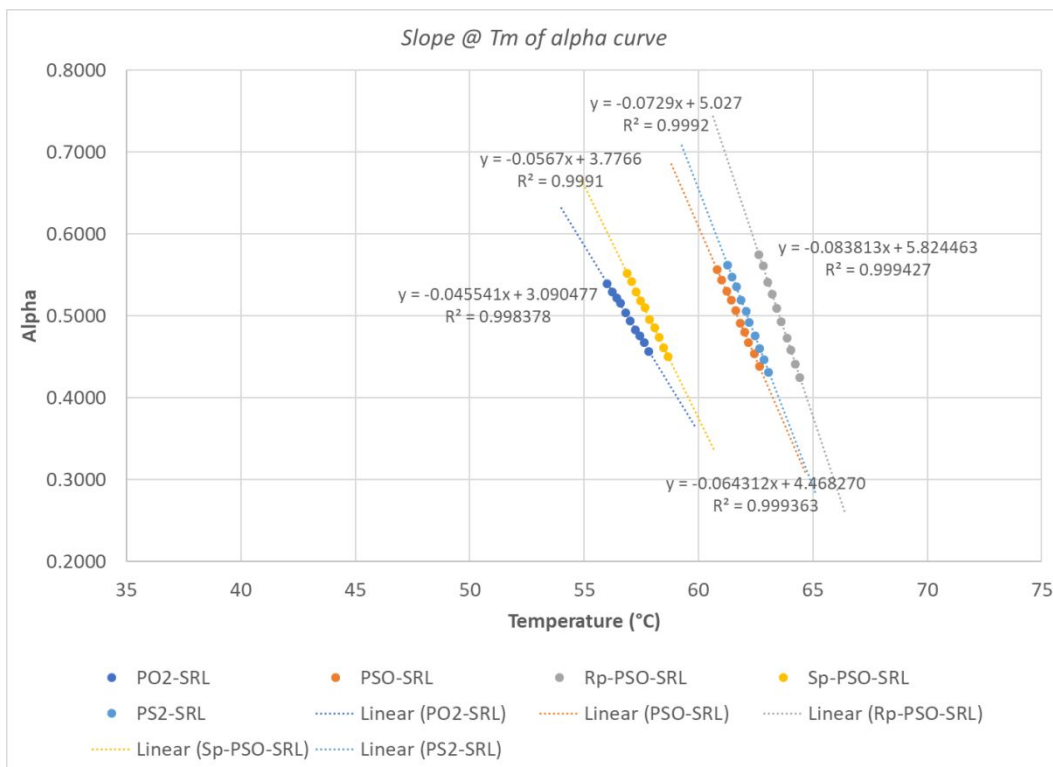**Figure S6.** Alpha curves.

Figure S7. Slopes at T_m values

Table S2. Calculation of thermodynamic parameters for RNA-SRLs (R=1.987207 cal/K*mol; C to K = 273.15; Temp. = 25°C).

PO2-a			PSO-a			Rp-PSO-a			Sp-PSO-a			PS2-a				PO2-SRL		
dalpha/dT (@ Tm)	-0.0455		dalpha/dT (@ Tm)	-0.0643		dalpha/dT (@ Tm)	-0.0838		dalpha/dT (@ Tm)	-0.0567		dalpha/dT (@ Tm)	-0.0729				Avg	StDev
Tm (from alpha curve)	330.05	K	Tm (from alpha curve)	334.85	K	Tm (from alpha curve)	336.65	K	Tm (from alpha curve)	330.95	K	Tm (from alpha curve)	335.25	K		ΔH	-41.0	1.4	kcal/mol
ΔH	-39.4	kcal/mol	ΔH	-57.3	kcal/mol	ΔH	-75.5	kcal/mol	ΔH	-49.4	kcal/mol	ΔH	-65.1	kcal/mol	TΔS	-37.0	1.2	kcal/mol
TΔS	-35.6	kcal/mol	TΔS	-51.0	kcal/mol	TΔS	-66.9	kcal/mol	TΔS	-44.5	kcal/mol	TΔS	-57.9	kcal/mol	ΔG	-4.0	0.2	kcal/mol
ΔG	-3.8	kcal/mol	ΔG	-6.3	kcal/mol	ΔG	-8.6	kcal/mol	ΔG	-4.9	kcal/mol	ΔG	-7.2	kcal/mol				

PO2-b			PSO-b			Rp-PSO-b			Sp-PSO-b			PS2-b				PSO-SRL		
dalpha/dT (@ Tm)	-0.0480		dalpha/dT (@ Tm)	-0.0679		dalpha/dT (@ Tm)	-0.0832		dalpha/dT (@ Tm)	-0.0593		dalpha/dT (@ Tm)	-0.0762				Avg	StDev
Tm (from alpha curve)	330.75	K	Tm (from alpha curve)	335.65	K	Tm (from alpha curve)	336.85	K	Tm (from alpha curve)	331.55	K	Tm (from alpha curve)	335.85	K	ΔH	-57.7	2.1	kcal/mol
ΔH	-41.8	kcal/mol	ΔH	-60.8	kcal/mol	ΔH	-75.0	kcal/mol	ΔH	-51.8	kcal/mol	ΔH	-68.3	kcal/mol	TΔS	-51.3	1.9	kcal/mol
TΔS	-37.7	kcal/mol	TΔS	-54.0	kcal/mol	TΔS	-66.4	kcal/mol	TΔS	-46.6	kcal/mol	TΔS	-60.6	kcal/mol	ΔG	-6.4	0.2	kcal/mol
ΔG	-4.1	kcal/mol	ΔG	-6.8	kcal/mol	ΔG	-8.6	kcal/mol	ΔG	-5.2	kcal/mol	ΔG	-7.7	kcal/mol				

PO2-c			PSO-c			Rp-PSO-c			Sp-PSO-c			PS2-c				Rp-PSO-SRL		
																	Avg	StDev
dalpha/dT (@ Tm)	-0.0481		dalpha/dT (@ Tm)	-0.0645		dalpha/dT (@ Tm)	-0.0853		dalpha/dT (@ Tm)	-0.0554		dalpha/dT (@ Tm)	-0.0748		ΔH	-75.9	1.2	kcal/mol
Tm (from alpha curve)	331.05	K	Tm (from alpha curve)	335.45	K	Tm (from alpha curve)	337.45	K	Tm (from alpha curve)	332.15	K	Tm (from alpha curve)	336.15	K	TΔS	-67.2	1.0	kcal/mol
ΔH	-41.9	kcal/mol	ΔH	-57.7	kcal/mol	ΔH	-77.2	kcal/mol	ΔH	-48.6	kcal/mol	ΔH	-67.2	kcal/mol	ΔG	-8.7	0.2	kcal/mol
TΔS	-37.7	kcal/mol	TΔS	-51.3	kcal/mol	TΔS	-68.2	kcal/mol	TΔS	-43.6	kcal/mol	TΔS	-59.6	kcal/mol				
ΔG	-4.2	kcal/mol	ΔG	-6.4	kcal/mol	ΔG	-9.0	kcal/mol	ΔG	-5.0	kcal/mol	ΔG	-7.6	kcal/mol				

			PSO-d													Sp-PSO-SRL		
																	Avg	StDev
			dalpha/dT (@ Tm)	-0.0646											ΔH	-49.9	1.7	kcal/mol
			Tm (from alpha curve)	335.55	K										TΔS	-44.9	1.5	kcal/mol
			ΔH	-57.9	kcal/mol										ΔG	-5.0	0.2	kcal/mol
			TΔS	-51.4	kcal/mol													
			ΔG	-6.4	kcal/mol													

			PSO-e													PS2-SRL		
																	Avg	StDev
			dalpha/dT (@ Tm)	-0.0611											ΔH	-66.9	1.6	kcal/mol
			Tm (from alpha curve)	336.35	K										TΔS	-59.4	1.4	kcal/mol
			ΔH	-54.9	kcal/mol										ΔG	-7.5	0.2	kcal/mol
			TΔS	-48.7	kcal/mol													
			ΔG	-6.2	kcal/mol													

4. Crystallization, X-ray data collection, phasing and refinement

Table S3. Selected crystal data, data collection and refinement parameters.

Crystal Data	PSO-SRL	PS2-SRL	S_p-MePO-SRL
Space group	$P4_3$	$P4_3$	$P4_3$
Unit cell constants a,b,c [Å]	29.64, 29.64, 76.66	29.59, 29.59, 76.51	29.34, 29.34, 75.66
Data Collection			
Wavelength [Å]	0.97857	0.97857	1.3418
Unique reflections	19,854 (1,896)[a]	18,152 (1,812)	18,805 (1,557)
Resolution [Å]	50.00-1.21 (1.25-1.21)[a]	30.00-1.25 (1.29-1.25)	27.36-1.20 (1.24-1.20)
Completeness [%]	99.2 (95.6)	99.5 (99.3)	94.1 (78.12)
I/σ(I)	37.32 (2.34)	40.06 (2.76)	23.47 (3.44)
R-merge	0.055 (0.538)	0.065 (0.510)	0.089 (0.658)
R-pim	0.028 (0.320)	0.028 (0.239)	0.021 (0.231)
Redundancy	4.6 (3.6)	6.0 (5.3)	17.0 (8.4)
Refinement			
R-work	0.173 (0.317)[b]	0.110 (0.148)[c]	0.177 (0.340)[d]
R-free	0.238 (na)[b]	0.140 (0.247)[c]	0.213 (0.364)[d]
Avg. B-factor, RNA [Å^2]	17.8	16.1	9.4
Avg. B-factor, water [Å^2]	32.9	17.7	19.5
R.m.s.d. bond lengths [Å]	0.01	0.02	0.007
R.m.s.d. bond angles [°]	2.4	2.5	1.3
PDB ID code	7JJD	7JJE	7JJF

[a] Numbers in parentheses refer to the outer shell.

[b] Outer shell for refinement is 1.26-1.21 Å.

[c] Outer shell for refinement is 1.28-1.25 Å.

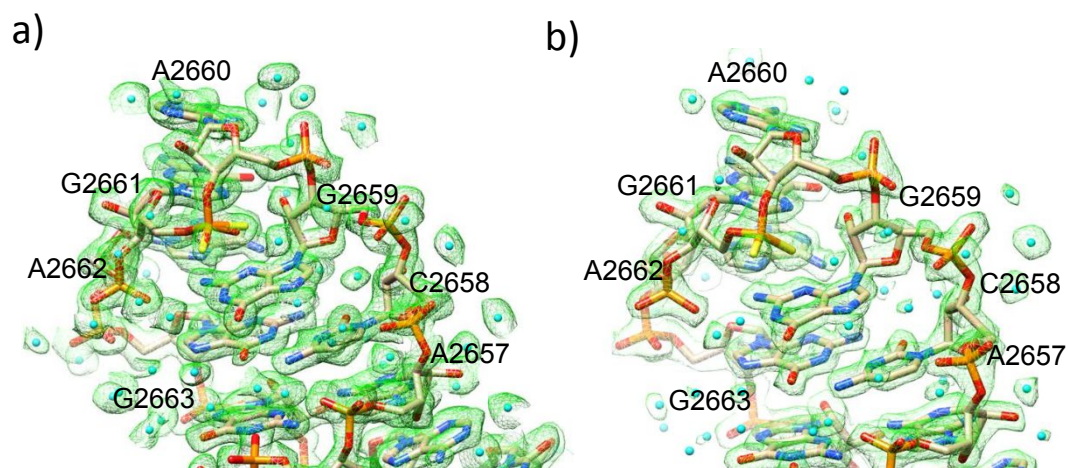[d] Outer shell for refinement is 1.24-1.20 Å.

Figure S8. Quality of the final 2Fo-Fc sum electron density (~1.1σ threshold) in the a) PSO-SRL and b) PS2-SRL structures. Water molecules are cyan spheres.

5. Thermodynamic measurements *continued*.

Figures S9-S12 and **Table S4,5** document the determination of T_m values and thermodynamic parameters for dAPO2- , dAPSO- and dAMePO-SRLs.
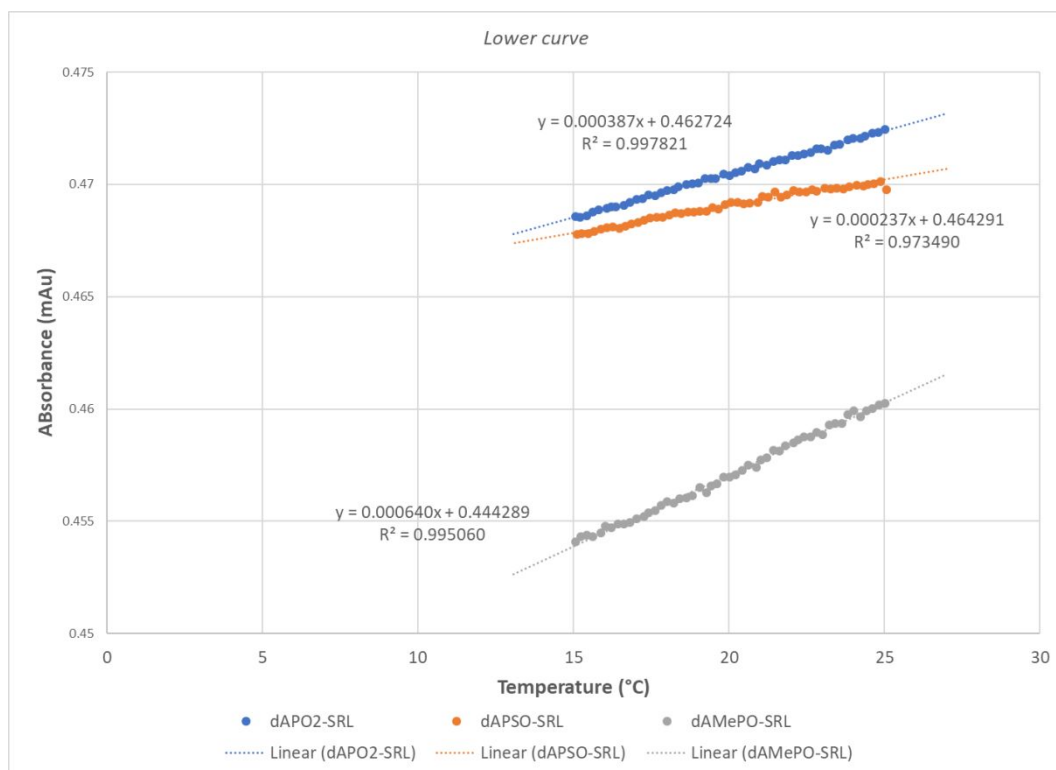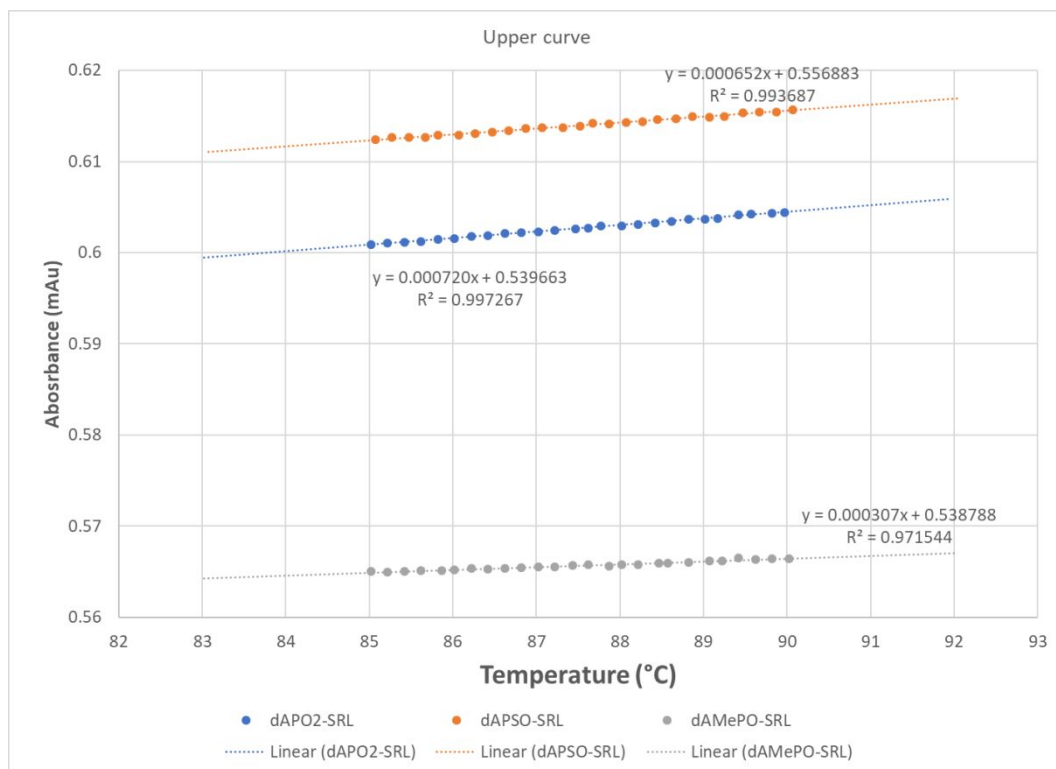

Figure S9. Lower baselines.
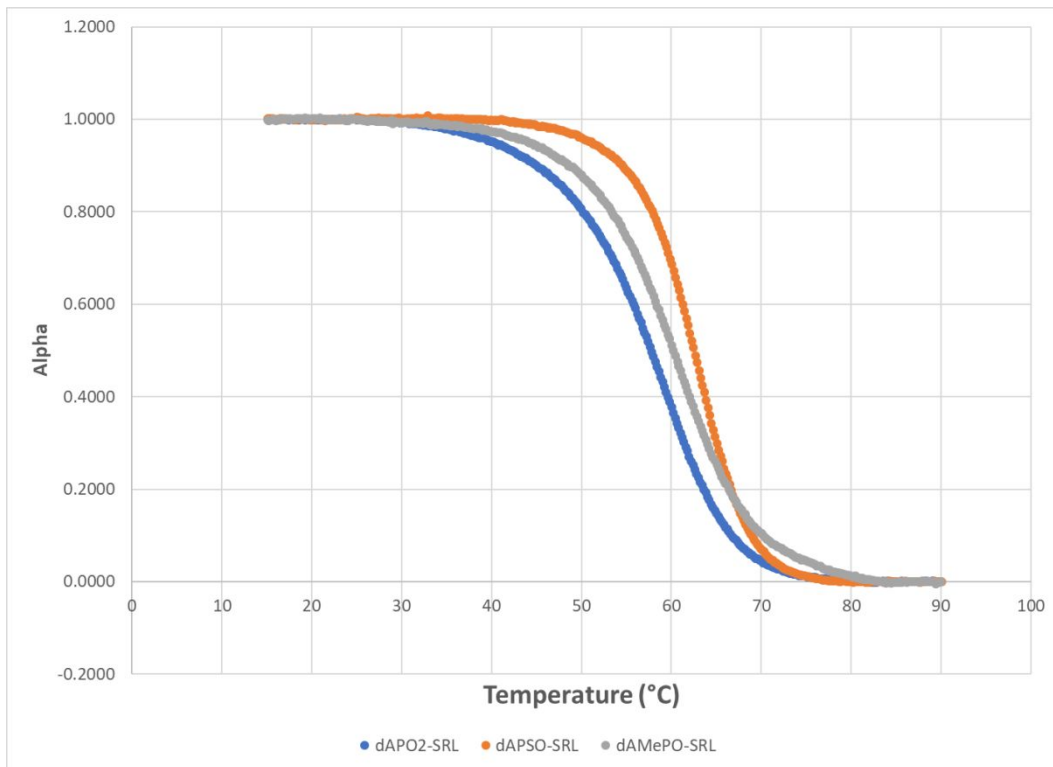

Figure S10. Upper baselines.

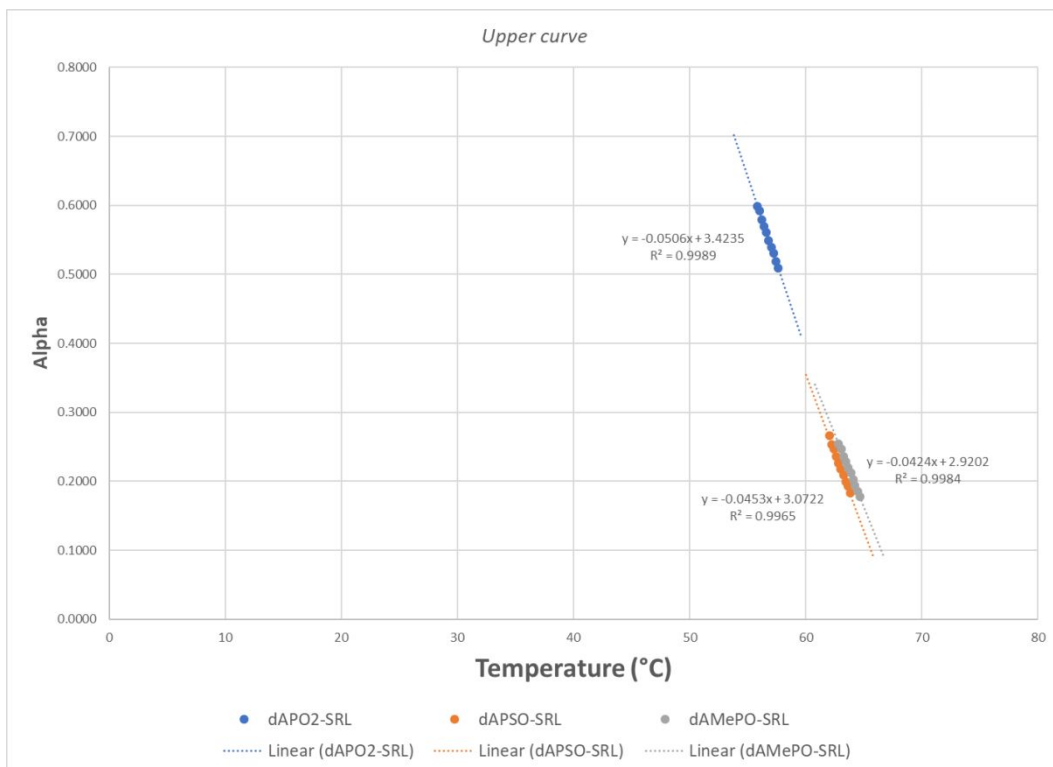**Figure S11.** Alpha curves.

Figure S12. Slopes at T_m values.

Table S4. Calculation of thermodynamic parameters for dA-SRLs (R=1.987207 cal/K*mol; C to K = 273.15; Temp. = 25°C).

dAPO2-a			dAPSO-a			dAMePO-a					dAPO2-SRL		
dalpha/dT (@ Tm)	-0.0538		dalpha/dT (@ Tm)	-0.0552		dalpha/dT (@ Tm)	-0.0563						
Tm (from alpha curve)	330.85	K	Tm (from alpha curve)	330.85	K	Tm (from alpha curve)	331.45	K				Avg	StDev
ΔH	-46.8	kcal/mol	ΔH	-48.0	kcal/mol	ΔH	-49.2	kcal/mol		ΔH	-48.0	1.2	kcal/mol
TΔS	-42.2	kcal/mol	TΔS	-43.3	kcal/mol	TΔS	-44.2	kcal/mol		TΔS	-43.2	1.0	kcal/mol
ΔG	-4.6	kcal/mol	ΔG	-4.7	kcal/mol	ΔG	-4.9	kcal/mol		ΔG	-4.8	0.2	kcal/mol

dAPO2-b			dAPSO-b			dAMePO-b					dAPSO-SRL		
dalpha/dT (@ Tm)	-0.0806		dalpha/dT (@ Tm)	-0.0846		dalpha/dT (@ Tm)	-0.0757						
Tm (from alpha curve)	335.75	K	Tm (from alpha curve)	335.15	K	Tm (from alpha curve)	336.45	K				Avg	StDev
ΔH	-72.2	kcal/mol	ΔH	-75.5	kcal/mol	ΔH	-68.1	kcal/mol		ΔH	-72.0	3.7	kcal/mol
TΔS	-64.1	kcal/mol	TΔS	-67.2	kcal/mol	TΔS	-60.4	kcal/mol		TΔS	-63.9	3.4	kcal/mol
ΔG	-8.1	kcal/mol	ΔG	-8.3	kcal/mol	ΔG	-7.8	kcal/mol		ΔG	-8.1	0.3	kcal/mol

dAPO2-c			dAPSO-c			dAMePO-c					dAMePO-SRL		
dalpha/dT (@ Tm)	-0.056		dalpha/dT (@ Tm)	-0.0568		dalpha/dT (@ Tm)	-0.0609						
Tm (from alpha curve)	333.25	K	Tm (from alpha curve)	332.85	K	Tm (from alpha curve)	333.35	K				Avg	StDev
ΔH	-49.4	kcal/mol	ΔH	-50.0	kcal/mol	ΔH	-53.8	kcal/mol		ΔH	-51.1	2.4	kcal/mol
TΔS	-44.2	kcal/mol	TΔS	-44.8	kcal/mol	TΔS	-48.1	kcal/mol		TΔS	-45.7	2.1	kcal/mol
ΔG	-5.2	kcal/mol	ΔG	-5.2	kcal/mol	ΔG	-5.7	kcal/mol		ΔG	-5.4	0.3	kcal/mol

Table S5. T_m values and thermodynamic parameters for SRLs with either a PO2 or a neutral MePO moiety linking dA2660 and G2661. T_m values for the isolated diastereomers is also reported.

SRL	T_m [°C]
dAPO2	59.8 ± 0.3
dAPSO	63.3 ± 0.2
dAMePO	60.4 ± 0.3
Sp-dAMePO (peak 1)	60.2 ± 0.3
Rp-dAMePO (peak 2)	60.6 ± 1.0